FOCUSED ULTRASOUND - A NEW FRONTIER IN THE NON-INVASIVE TREATMENT OF BRAIN DISEASES

by
Tarana Parvez Kaovasia

A thesis submitted to Johns Hopkins University in conformity
with the requirements for the degree of Master of Science in Engineering

Baltimore, Maryland
May 2021

Abstract

Focused ultrasound has been gaining impetus in the non-invasive treatment of different diseases. This includes various cancers, essential tremor, and Parkinson's disease, to name a few. The ability of focused ultrasound to concentrate energy at a single focal point away from the surface of the transducer allows for therapies to reach a targeted region in a non-invasive manner.

Of the different diseases that can be treated using focused ultrasound, brain morbidities have been garnering special interest in ongoing research. This can be attributed to focused ultrasound being able to access any area of interest in the brain (for example, a tumor), without the risk of disturbing surrounding critical structures. In this thesis, we discuss the application of focused ultrasound for the treatment of various brain diseases. We also look at the development and use of preclinical instrumentation for advancing novel therapies in animal models to clinical translation.

Since focused ultrasound involves the deposition of energy at the target region in the brain, care must be taken that there are no downstream effects of these therapies on the central nervous system. Change in the cerebrospinal fluid (CSF) pressure is an example of an important effect that may be seen as a result of focused ultrasound-based therapies, a change which could cause detrimental effects of its own. Here, we also look at the development and potential use of a fiber-optic based sensor to monitor CSF pressure in the central nervous system before, during, and after focused ultrasound-based therapies.

Thesis Readers

Dr. Amir Manbachi (Co-Primary Advisor)
Assistant Professor
Department of Neurosurgery, Biomedical Engineering, Electrical and Computer Engineering
Johns Hopkins University

Prof. Betty Tyler (Co-Primary Advisor)
Associate Professor
Department of Neurosurgery
Johns Hopkins University

Dr. Michael Caterina
Solomon H. Snyder Professor
Director, Neurosurgery Pain Research Institute
Interim Director, Department of Biological Chemistry
Professor of Neurosurgery
Professor of Biological Chemistry
Professor of Neuroscience
Johns Hopkins University

Success is the ability to go from one failure to another with no loss of enthusiasm.

- Winston Churchill

Acknowledgements

'Teachers have three loves: the love of learning, the love of learners, and the love of bringing the first two loves together'. Dr Manbachi and Prof. Tyler, thank you for introducing me to the field of focused ultrasound, and for sharing your wealth of knowledge with me. You both were not only always receptive to my ideas, but also helped me plan my way through them.

I am grateful for every single member of the two labs I call home at Hopkins - the HEPIUS Lab and the Hunterian Neurosurgical Laboratory. I would like to thank Desmond Jacob and Dr Marie-France Penet at the Department of Radiology for the long hours spent in the MRI room, and Dr Marc Santos and Dr Rajiv Chopra at FUS Instruments for their patience in helping us debug and better understand the RK-300. I would also like to thank George Coles and Austin Devinney from the Johns Hopkins Applied Physics Laboratory with their assistance with the pressure sensor testing. It truly does takes a village. I would especially like to thank Molly Acord for being my partner in crime, matching my energy, and weathering the storm with me. I will forever cherish our friendship and am grateful to have worked with you.

I would like to acknowledge our funding sources - the Department of Neurosurgery (Johns Hopkins School of Medicine), and the Defense Advanced Research Projects Agency, DARPA, Award Contract : N660012024075.

I would like to thank the Department of Biomedical Engineering for a rich curriculum, and the faculty for teaching it with such vigor that it not only expanded my

knowledge-base, but also strengthened my love for Biomedical Engineering.

Finally, I would like to thank my family. Thank you for believing in me, and for being there every step of the way despite the nine hours between us.

I hope I have made you all proud.

Contents

List of Tables

List of Figures

Chapter 1

Introduction

Focused Ultrasound (FUS)

Acoustic waves with frequencies above the human audible range, that is, 20kHz are referred to as ultrasound. In the field of medicine, ultrasound is broadly used in imaging and therapy. When used in imaging (sonography), a transducer (piezo-electric crystals that vibrate, causing the medium in contact with it to vibrate at the same frequency) emit ultrasonic waves in the frequency range of 2 to 18 MHz. A receiver located near the transducer picks up waves reflected from the tissue being imaged and converts it into an electrical signal [1]. Sonography should cause no physiological effects during its application. Therefore, the Food and Drug Administration (agency responsible for public health) allows the use of 'diagnostic' ultrasound within certain acceptable limits, as listed in the paper by Nelson et al [2].

During focused ultrasound (FUS), acoustic waves are generated by a transducer. The transducer(s) is designed to converge these acoustic waves at a focal point, which is often at the target tissue location. The focal point is where the transducer generates its maximum acoustic energy [3]. This acoustic energy can be used in a variety of different therapeutic applications. Focused ultrasound can be used to carry out thermal ablation, blood brain barrier opening, histotripsy, sonodynamic therapy, radiosensitization, or immunomodulation (Figure 1-1) [4].

One of the biggest advantages of focused ultrasound-based therapies is that it can be used to non-invasively access a target structure in the body. The potential to access structures of interest without disturbing surrounding eloquent brain matter is what has drawn huge interest to this therapeutic modality.

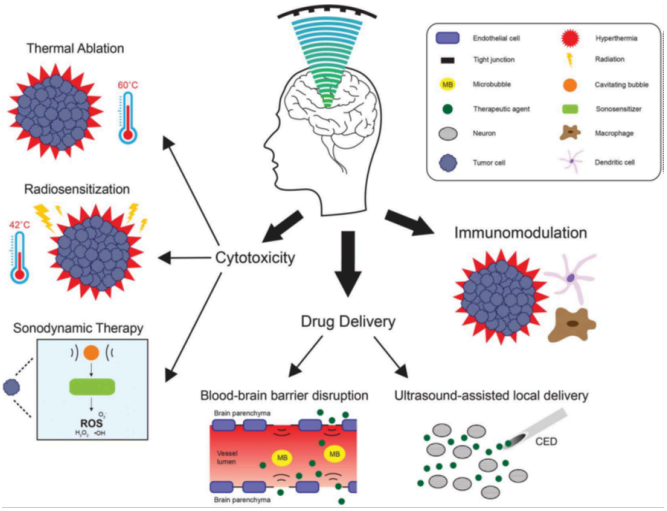

Figure 1-1. FUS Applications: some therapeutic effects achievable in the brain (reproduced with permission from [4])

Understanding focused ultrasound terminology and parameters

Before we dive into the focused ultrasound and its applications, let us understand the parameters that govern focused ultrasound treatments (visualized in Figure 1-2):

- **Frequency**: is the number of ultrasound waves generated by the transducer per second. It is also the rate at which the molecules of the medium coupled with the transducer vibrate.
- **Burst Length**: is the time duration for which the transducer is active and emitting acoustic energy.
- **Inter-pulse Interval**: is the period of rest between two successive bursts.

- **Pulse Repetition Interval**: is the sum of the burst length and inter-pulse interval.
- **Duty Cycle**: is the ratio of the burst length to the pulse repetition period. It signifies the percentage of time the transducer is active.
- **Time Duration**: This is the total duration for which the ultrasound transducer will sonicate. It consists of a burst followed by an inter-pulse interval followed by a burst, repeated in succession.

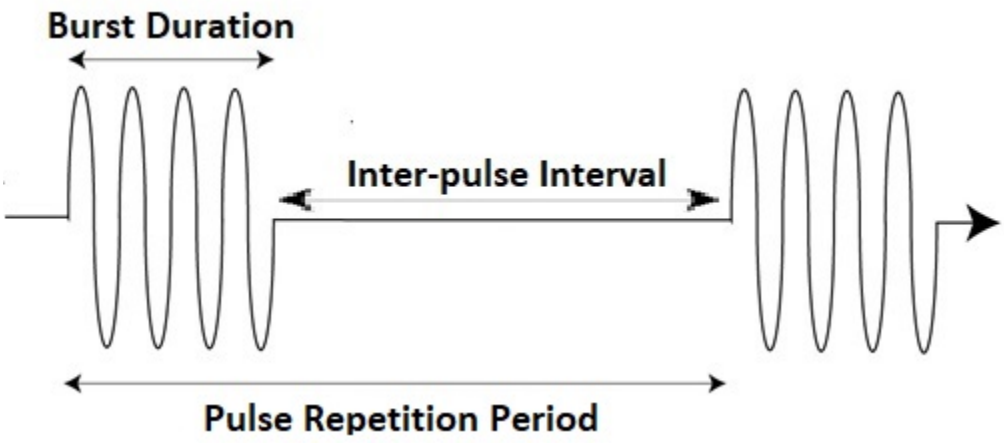

Figure 1-2. Ultrasound parameters

Now, with the basic understanding of focused ultrasound and its accompanying parameters, the different applications of focused ultrasound can be explored.

Applications of Focused Ultrasound in Neurology

Blood-Brain Barrier Opening

The blood-brain barrier (BBB) is a lining of packed endothelial cells along the blood vessels in the brain which form tight junctions. It only allows the exchange of small molecules (nutrients, oxygen, and waste) between the cerebrospinal fluid and the blood [5]. Drugs that are used in the treatment of brain tumors (chemotherapy),

Alzheimer's disease, or Parkinson's disease are typically too large in size to cross the BBB [6]. Therefore, in order to allow drugs to reach the target tissue in the brain, the BBB needs to be opened. However, this opening cannot be permanent to ensure that after the drug is delivered, the BBB can return to performing its functions.

The BBB can be transiently opened at the site of the target structure to allow passage of drug molecules. Different methods are being investigated for this purpose. These include ultrasound, photochemical internalization, photodynamic therapy, and osmotic opening. Of these, focused ultrasound is the most widely researched method [7, 8].

Focused ultrasound in conjunction with microbubbles (eg: Optison™, Definity) are used to reversibly open the BBB without causing damage to the parenchymal cells [9]. The microbubbles, which are micron-diameter shells filled with gas, are injected intravenously and ultrasound applied transcranially. At the beam focus, the acoustic waves cause the microbubbles to vibrate, and their ultimate cavitation in turn opens the BBB at the target site. The drug is then delivered intravenously as a bolus. Due to the inherent nature of the BBB, it closes as early as 6 hours after the application of focused ultrasound, when optimal parameters are used [10].

Previous studies on animals, both mice and rabbits, have used MRI to guide the ultrasound and, with the help of contrast agents, to image the BBB opening. These studies have shown the successful opening and closing of the BBB. Studies have also shown the increased amounts of drugs being delivered to the tumor site through the open BBB when compared to sham procedure controls. Minimum damage to surrounding tissue from the ultrasound, microbubbles, or drugs were also verified [11–15].

Human studies have been performed with considerable success [16]. From 2015-19, Kullervo et al. [17] conducted a feasibility and safety study to treat primary brain tumors in humans using this method. This study was conducted with 5 patients with

gliomas who had not received any previous treatment. They received the treatment, that is, liposomal doxorubicin (1 patient) or temozolomide (4 patients) a day prior to their scheduled surgical resections. Focused ultrasound was used to open the BBB to provide these agents access to the tumor. The BBB opening was visually confirmed via MRI scans facilitated by contrast agents. Histological analysis of the tumor and peritumor sample obtained during resection showed the presence of the drug in the treatment group. None of the patients suffered adverse effects.

Ablation

Extremely high (hyperthermia) or low (hypothermia) temperatures, when applied to tissue, can result in death, also known as necrosis. Temperatures below -41°C and above 60°C result in instantaneous necrosis for most cell types. Thermal ablation is aimed at killing the entire tumor mass along with a 5-10 mm margin of surrounding normal tissue in situ. Over the course of several months, the body can then absorb this necrotic mass [18].

High Intensity Focused Ultrasound (HIFU) is one of many methods available to perform thermal ablation [18]. During HIFU, the acoustic waves converge at a focal point, which is often at the tumor location. The acoustic energy at the focal point is absorbed by the tissue, resulting in heat generation. Therefore, lesions are formed by coagulation necrosis due to the extreme state of hyperthermia at the focal point [19].

To cause tissue temperatures to be at least 60°C at the focal point *in vivo* in the presence of the human skull, the frequency of the ultrasonic wave should be at least 650 kHz [20]. The human skull is considerably thick [21], and significantly attenuates waves of frequencies required to perform thermal ablation [22]. Therefore, if ablation using HIFU is to be carried out *in vivo*, high power would be required to allow the acoustic wave to propagate through the skull. This would result in the skull absorbing these attenuated waves and heating up considerably [23] making non-invasive thermal

ablation using focused ultrasound significantly hard to achieve.

Therefore, research into minimally invasive techniques to facilitate thermal ablation using focused ultrasound is currently underway. Manbachi et al. [24] designed an ultrasound-guided focused ultrasound transducer to be placed inside the BrainPath, which is used to gain atraumatic access to regions of the brain. The BrainPath trocar could be placed in a relatively insensitive area of the brain and the transducer could be used to ablate the tumor from a distance, potentially bypassing sensitive tissues. Successful *in vitro* studies were performed and will be followed up by cadaveric studies. Canney et al. developed an MRI-guided 56 element interstitial ultrasound applicator to ablate both primary and secondary brain tumors. *In vitro* studies were performed with tissue-mimicking phantoms along with simulations to demonstrate the efficacy of the device [25]. Despite non-invasive ablation being extremely hard to achieve, Werner et al. performed [20] the first non-invasive thermal ablation of a glioblastoma tumor using transcranial focused ultrasound in 2014, significantly reducing the tumor volume. In this study temperatures lower than 60°C were achieved causing coagulation over time instead of instantaneously, thus increasing sonication time.

Histotripsy

There are nano-sized gas pockets that exist throughout our body. When focused ultrasound of very high pressure is applied to tissue, these naturally-occurring nano-sized air pockets expand and collapse in rapid succession, forming a bubble cloud. This phenomenon is known as cavitation [26]. When cavitation occurs, the cells in the vicinity experience high amounts of shear stress. If this shear stress experienced is above the intrinsic threshold for a sufficient duration of time it can cause cell destruction [27]. After destruction, the cellular debris is cleared out by the body within 2 weeks. This process of controlling cavitation mechanically to ablate target tissue is known as histotripsy [28].

Since histotripsy involves cellular destruction at the site of the bubble cloud formation, the boundaries of the resulting lesion formation are unlike thermal ablation (i.e. thermal spread causes irregular boundary formation) [29]. Since histotripsy involves sonications with very high power but a small duty cycle, the heating of the skull can be minimized, and it can therefore be used in the brain as a completely non-invasive therapy.

Additionally, the cellular debris formed has been shown to elicit an immune response. This could not only help prevent recurrence of the tumor, but also shrink metastatic tumor masses (discussed in detail below in Immunomodulation).

Histotripsy is currently in clinical trials for the treatment of liver tumors [30]. Research for translation of its application to treat brain tumors is underway. The main goal of the research is to optimize histotripsy parameters, such as correcting for aberrations caused due to the presence of the skull, using imaging modalities to guide the treatment, and selectively sensitizing the tumor tissue (nano-particle mediated histotripsy), for future treatment procedures in the brain [31, 32].

Immunomodulation

Immunotherapy involves treating a disease by suppressing or activating the immune system, and has been heavily investigated in the field of cancer research [33]. For tumors that recur, the need for tumor-specific antigens is great. Focused ultrasound demonstrates the potential to cause an immune response to prevent recurrences by inducing tumor-specific antigens.

Focused ultrasound performed with parameters causing mechanical lysis or thermal coagulation of tumor cells primarily results in the release of danger signals known as heat shock protein 60 (hsp60) and adenosine triphosphate (ATP), as seen in an *in vitro* study performed by Hu et al [34]. The release of these signals was five times greater for mechanical HIFU (histotripsy) than thermal HIFU. This is because the thermal

HIFU parameters elicited thermal necrosis of tumor cells primarily causing the release of these danger signals. However, this release was stable throughout and did not progress as treatment continued. Additionally, the maturation of antigen-presenting cells (APCs) due to these released danger signals was much more evident in histotripsy than thermal ablation. This shows promise that the FUS-induced immune response of cancer cells can be used as a prevention for the recurrence of brain tumors (i.e., glioblastoma multiforme).

Radiosensitization

Radiation therapy (RT) uses high doses of radiation to kill cancer cells and to slow tumor growth by destroying its DNA [35]. Radiation is part of the clinical treatment regimen in brain tumor treatment. Radiation in combination with hyperthermia (HT) has been investigated due to the increased sensitization to radiation under such conditions [36]. Unfortunately, the only way to achieve hyperthermia in the tumor region was via invasive heat probes. Due to its invasive nature, RT+HT was less popular than other cancer therapies (for example: surgical resection, chemotherapy) [37]. Due to the advancements in focused ultrasound technology, there is new interest in radiosensitization, as FUS can be applied transcranially to increase tumor temperature to hyperthermia requirements (42°C). There are several processes believed to explain how HT increases the efficacy of radiation. Previous studies have shown that HT increases perfusion and oxygenation in/around the tumor, activates immune response, causes cell death, and most importantly, reduces the ability for the cancerous DNA to repair itself [35].

Sonodynamic Therapy

Glioblastoma multiforme (GBM) is the most common malignant primary brain tumor. The tumor is aggressive, invasive, and infiltrating in nature, which also leads

to one of the shortest survival rates among cancers. The average survival is 12-15 months and only about 11% of patients survive 5 years. Due to the microstructures GBM develops, total surgical resection is difficult, leading to a high recurrence rate. [38]

A promising treatment for GBM involves the use of a sonosensitizing agent which becomes cytotoxic to malignant tumor cells once exposed to focused ultrasound, otherwise known as sonodynamic therapy (SDT). For brain tumors, especially GBMs, 5-aminolevulinic acid (5-ALA) has been investigated as a sonosensitizing agent [39]. 5-ALA is a naturally occurring intermediate in the pathway by which heme is synthesized, and when orally administered to GBM patients, it acts like a pro-agent that accumulates in gliomas and within surrounding cancer cells outside the tumor bulk [40]. GBMs become highly vascularized by sprouting new capillaries from pre-existing vessels, significantly affecting the BBB within their region, and ultimately allowing for GBM uptake of 5-ALA [41]. 5-ALA is preferential taken up GBM cells [42–44]. Once inside GBM cells, 5-ALA is converted to fluorescent protoporphyrin (PpIX), which allows it to be regularly used in guided resection surgeries for visualization purposes [45].

There are eight enzymatic steps involved in the heme pathway (biochemical pathway responsible for heme synthesis in blood [46]) between the mitochondria and cytoplasm. CPgenIII is a product of the fifth enzyme, uroporphyrinogen III decarboxylase, and it enters the mitochondria from the cytoplasm to serve as the immediate precursor for PpIX. This process is energy-dependent, so CPgenIII movement requires an ATP-binding cassette transporter: ABCB6. GBM cells have been shown to possess significantly greater levels of ABCB6 than healthy cells [42–44, 47, 48]. The mechanical interaction of ultrasound and PpIX within the tumor causes the generation of reactive oxygen species (ROS), producing direct cytotoxicity in malignant cells [49].

There are several benefits of SDT over thermal ablation when it comes to treating

GBM. One being that little to no temperature rise in the tissue is needed. The production of ROS means that FUS is not needed to produce elevated temperature values, which are typically required for hyperthermia and ablation treatments [4]. Therefore, far less energy is required for SDT and there is minimal risk for patient scalp overheating (a common side effect of brain tumor ablation) [24, 49]. Another advantage of SDT over ablation is that it does not need to be pulsed, meaning the procedure can be continuous and faster. In addition, due to the unwanted heating of the skull, ablation is usually limited to tumors in the center of the brain, whereas, SDT is feasible for tumors located in any part of the brain.

Comparing Focused Ultrasound Applications with Each Other and Current Clinical Treatments

When it comes to treating brain tumors, there are three conventional standards of care - surgical resection, chemotherapy, and radiation therapy. Surgical Resection, although invasive, is a preferred form of therapy with the aim of removing the entire tumor volume. However, surgical resection is limited by the location of the tumor. The presence of surrounding eloquent structures may prevent surgical access to the tumor. Additionally, surgical resection may not remove all of the tumor micro-structures, causing the tumor to recur [50]. Therefore, non-invasive therapies are either used in conjunction with or in place of surgical resection. This commonly includes chemotherapy and radiation therapy. As previously described, most chemotherapeutic drugs used to treat brain tumors are prevented by the BBB from reaching the tumor in the brain [51]. Radiation therapy, although able to reach the tumor site non-invasively, poses a risk of harming healthy cells and causing multiple, undesired side-effects.

These drawbacks of conventional therapies allow focused ultrasound to be investigated for the treatment of brain tumors. Thermal ablation and histotripsy can be used to perform 'non-invasive resection'. The end-goal of these two applications

would be to kill the entire tumor mass (including the micro-structures) while trying to minimize collateral damage. In cases where one wishes to explore the efficacy of chemotherapeutic drugs on the tumor before considering resections, BBB disruption to aid chemotherapy shows promise. SDT shows promise for preferentially killing tumor cells while sparing healthy cells, especially at the tumor border where micro-structures exist in such close proximity to the healthy cells.

Although focused ultrasound research is continually progressing in the field of neuro-oncology, it also is being utilized for treating other neurological diseases, like Alzheimer's disease, Parkinson's disease, and essential tremor. Focused ultrasound has been FDA approved to treat essential tremor non-invasively by ablating the ventral intermediate nucleus in the thalamus [52]. Focused ultrasound has also been approved to open the BBB for the treatment of Parkinson's disease [53]. The FDA has also approved clinical trials for blood-brain barrier opening to treat Alzheimer's disease and even tumors [54]. Overall focused ultrasound shows great promise for the safe and efficacious treatment of neurological diseases.

Potential Downstream Effects of Focused Ultrasound

Focused ultrasound is an exciting field of research - with all its current and potential benefits. However, care must be taken to ensure that there are no undesirable side effects of these focused ultrasound-based treatments. This is especially critical in brain applications because there is close to zero tolerance for collateral damage.

Overheating of the skull

Thermal ablation using focused ultrasound requires appreciable power to be delivered at the focus point continuously (100% duty cycle) to allow tissues to reach an instantaneous coagulation temperature of 60°C. In "transcranial" focused ultrasound, this energy has to pass through the skull, and as previously discussed, the skull heavily

attenuates ultrasound waves, by absorbing them. The ultrasound energy that is absorbed by the skull during thermal ablation can cause considerable heating of the skull and tissues within the vicinity of the skull [22, 23].

Therefore, ablation of tumors generally requires a portion of the skull that lies in the ultrasound beam path to be removed (by performing a craniotomy). If this craniotomy is not performed, then the power delivered to the focus would need to be reduced (to prevent heating of the skull). Under these circumstances, the tissue would not be able to reach 60°C quickly and therefore the time taken for the tissue to coagulate would be longer. This would cause the treatment duration to increase considerably [20].

Additionally, by leaving the skull intact, only centrally located tumors can be treated. This is because energy increases closer to the focal spot. For tumors near the skull, the focus would be required to be formed closer to the skull. This would cause a higher degree of heating of the skull, and therefore, increase the chances of damaging the skull and surrounding tissue [55].

Killing healthy tissue

In applications of focused ultrasound that cause direct death of structures in the brain (for instance, brain tumors), care must be taken to monitor and minimize collateral damage, that is, damage to healthy brain cells and tissues.

In thermal ablation, when the targeted tissue is heated, the thermal energy generated at the focal spot can diffuse outwards, an effect known as thermal spread [56]. This causes lesions with irregular boundary shapes [24, 56]. Care must be taken that this thermal spread does not encroach upon and kill healthy tissue in the brain.

In histotripsy, since focused ultrasound-induced cavitation is used to kill cells in the target structure, the boundaries of the lesion are sharp (unlike thermal ablation). However, in an attempt to, for example, mechanically kill all the tumor cells in a

tumor (to prevent recurrence), the bubble-cloud might be brought precariously close to healthy tissue at the tumor margin, therefore risking collateral damage.

In sonodynamic therapy, the reactive oxygen species that cause cell death are produced intracellularly [57]. It is still unclear whether the reactive oxygen species that are produced, during cell disruption, can diffuse out and extracellularly cause cell death. If so, care must be taken especially at the tumor margins.

Increasing cerebrospinal fluid (CSF) pressure

Since focused ultrasound involves delivering energy to a targeted location in the brain, care must be taken to ensure that it does not cause any major changes systemically in the brain or spinal cord. One important parameter that should be monitored for changes is the cerebrospinal fluid pressure. This is discussed in depth in Chapter 3.

Chapter 2

Focused Ultrasound Instrumentation for Preclinical Studies

Small animal studies are a vital step in translating focused ultrasound - based treatments to the clinic. For "non-neuro" therapeutic applications of focused ultrasound, ultrasound imaging can be used to guide the therapy in real time. For transcranial focused ultrasound applications in the brain, ultrasound imaging cannot be used because of the presence of the skull (which heavily attenuates acoustic waves). Therefore, Magnetic Resonance Imaging (MRI) can be utilized as an imaging modality to guide focused ultrasound therapies in the brain. Although it is not as immediate as ultrasound [58], MRI allows for high resolution imaging of brain anatomy to guide targeting of the structure of interest. It can also be used to view the therapeutic effects of focused ultrasound both during and after treatment.

In order to employ MRI as an imaging modality in focused ultrasound treatments, the focused ultrasound system, at least the transducer and guiding system, should be MRI-compatible.

The RK-300 by FUS Instruments

The RK-300, developed by FUS Instruments, is an MRI-guided Focused Ultrasound System that can be used to perform small animal studies including BBB opening, sonodynamic therapy, ablation, and neuromodulation.

The RK-300 in the Department of Radiology (Johns Hopkins School of Medicine), can be broken down into three subsystems - Hardware, Software, and Accompanying Components. The following sections briefly describe these three subsystems.

Hardware

The hardware can be divided into the front-end and back-end. The front-end is the RK-300 arm (Figure 2-1.b) which consists of a single element transducer with a center frequency of 1.0106 MHz. The concave surface of the transducer results in the focus being geometrically fixed. The calculation of the focal distance for the transducer on the RK-300 is shown in Figure 2-2. The concave surface is the transducer and the apex of the right-angle triangle is the focus.

The focus is an ellipsoid that has a long axis around 9.3 mm in the direction of ultrasound propagation and a short axis of 1.7 mm perpendicular to the direction of ultrasound propagation (measured with a hydrophone). Changing the frequency changes the spatial extent of the elliptical focal region, but the focus itself remains centered at the geometric center (calculated in Figure 2-2) of the spherical cap transducer. This information was provided through correspondence with the company.

The positioning system also located on the arm consists of two motors that mechanically steer the focus by physically moving the transducer. In addition to the transducer and motor, the arm is designed to support a small animal under anesthesia and maintain its vitals during the study.

The back-end consists of the driving electronics shown in Figure 2-1.a. The RK-300

arm goes into the bore of the MRI, while the driving electronics stay outside of the MRI room.

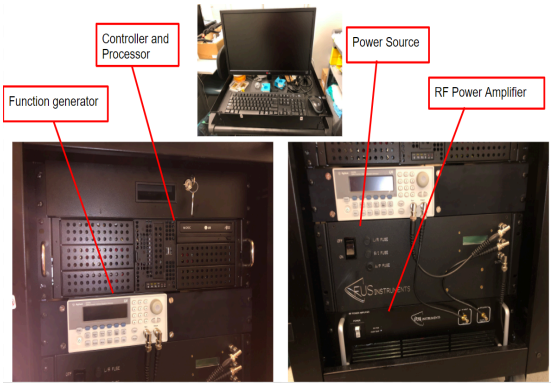

(a) Driving Electronics (Back-End)

(b) The RK-300 Arm

Figure 2-1. The RK-300 at Johns Hopkins

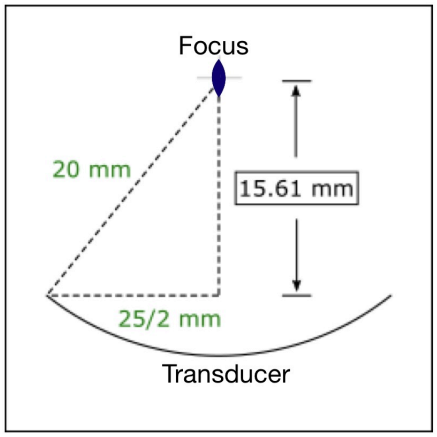

Figure 2-2. Transducer and Focus Geometry

Software

The software, which provides a User Interface (UI) to the entire system, runs on a PC (shown in Figure 2-3). Through this UI, the focus is registered and sonication is performed with the desired parameters in the desired target location(s).

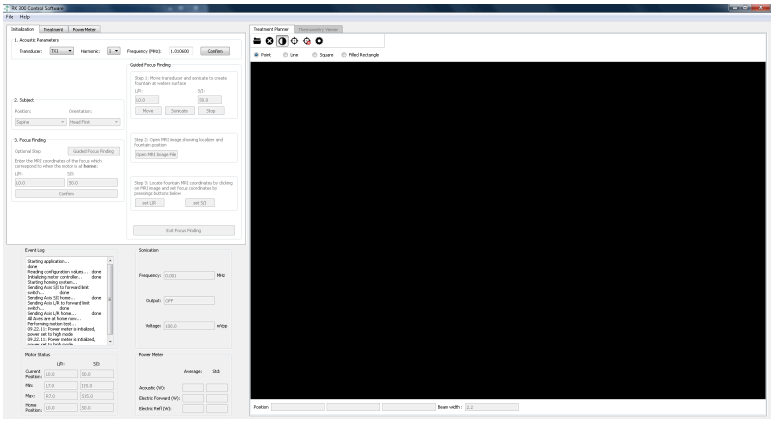

Figure 2-3. User Interface of the Software

Accompanying Components

The following components accompany the system, and serve as accessories to a particular task performed:

- Plastic sledge (Figure 2-4.a): Covers the transducer cavity, and serves as the bed on which the phantom/animal can be placed.
- Membrane cuboid (Figure 2-4.b): The plastic sledge has a rectangular window over the transducer to allow for the propagation of ultrasound. The membrane cuboid is a coupling medium that covers this window to prevent water (that fills the transducer cavity) from spilling while allowing the ultrasonic waves to pass through.
- Bath (Figure 2-4.c): This is used in the process to register the focus.
- Focal marker (Figure 2-4.d): Appears hypointense (dark) in T1-weighted FLASH MRI scans, and is used in the process of registering the focus.

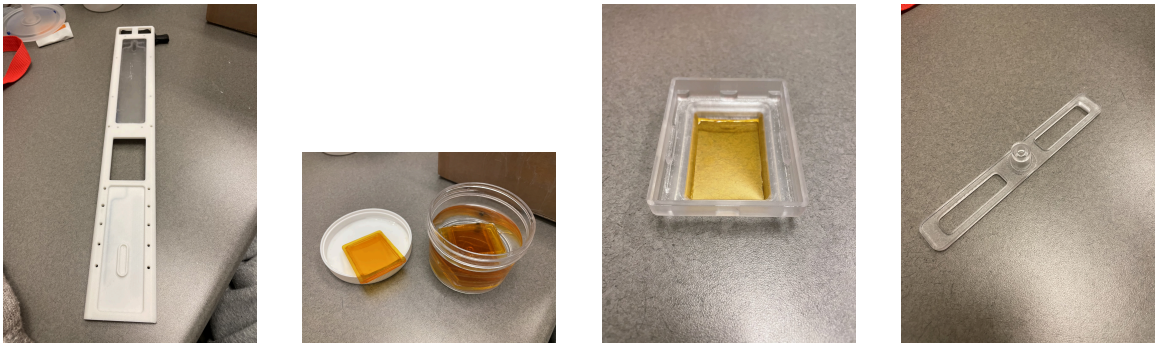

(a) Sledge **(b)** Membrane **(c)** Water Bath **(d)** Focal Marker

Figure 2-4. Accompanying Components

Experimental Design

The main aim of the experiment was to observe focus formation at the target using the RK-300. To achieve this, an experiment was designed to focus ultrasound in a solid water phantom.

Initial System Setup

The front-end was connected to the back-end of the system using a zero insertion force (ZIF) connector. After ensuring the 1.0106 MHz impedance matching circuit was connected, the system was turned on.

The hardware was then powered up, and the software was opened. One of the first subsystems that the software checked was the motors that are used to perform mechanical focus steering. The motors were visually observed to move the transducer and settle into its home position. After the transducer settled into its home position, the plastic sledge was attached. The transducer cavity was then filled with degassed water ($<$ 1 ppm of dissolved oxygen) up to the window opening. The membrane cuboid was then placed over this water-filled transducer cavity (Figure 2-5). The absence of air bubbles in the cavity was then visually confirmed.

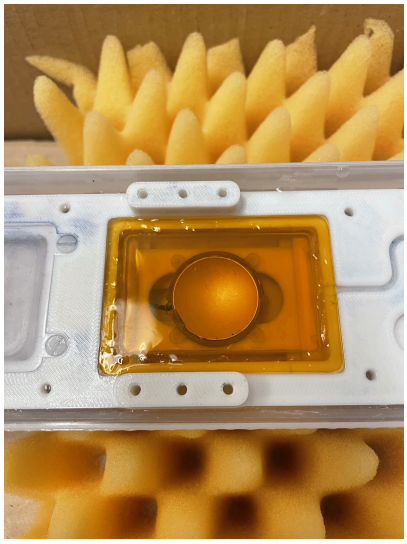

Figure 2-5. Membrane placed over the window of the bath filled with water

Registering the Focus

The main purpose of this step was to register the focus of the RK-300 (while the transducer is in its home position) to the MRI. This means that the focus of the transducer is recorded in MRI coordinates, and this is used to calculate relative traveling distance to new target coordinates during treatment.

After ensuring the absence of air bubbles, a layer of degassed water was placed over the membrane cuboid. The water bath was then slid over this layer of water. Once again, the absence of air bubbles throughout the coupling path was ensured. The bath was then filled with degassed water. In the software's "Initialization Tab" (Figure 2-6):

1. Under "Acoustic Parameters":
    - The transducer (TX1) was selected
    - A harmonic frequency of 1 was selected. The corresponding frequency of 1.106 MHz was reflected under "Frequency (MHz)"
2. Under "Focus Finding":

- "Guided Focus Finding" was selected
- To the right, under "Step 1", the sonicate option was selected.

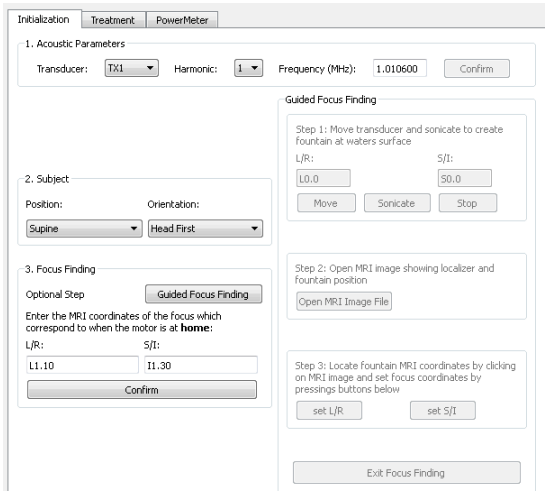

Figure 2-6. Registration Software Initialization Tab

After setting these parameters, a water fountain appeared on the surface of the water in the bath. This corresponded to the focal region being formed by the transducer. The water level was then adjusted until the sharpest focus, that is, the narrowest fountain was observed (Figure 2-7.a). The focal marker was then placed over the fountain, taped down, and the bath was filled with degassed water until there was water in almost the entire column of the focal marker (Figure 2-7.b).

The prepped RK-300 arm was then placed into the bore of the MRI (with an imaging coil in place). Care was taken not to spill water out of the water bath, and the back-end was kept outside the MRI room.

The center of the water column of the focal marker was placed at the isocenter of the magnet. Three-plane localizer images were acquired to ensure optimal positioning and confirm the water level in the column. Coronal T1w FLASH scans were then acquired. The parameters of the scan are provided in Table 2-I.

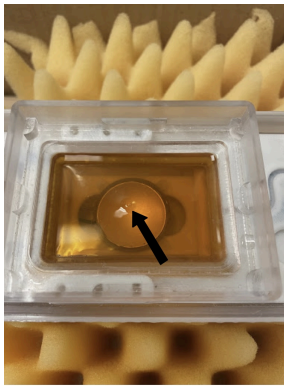

(a) Focus forms a small fountain in the water bath (black arrow)

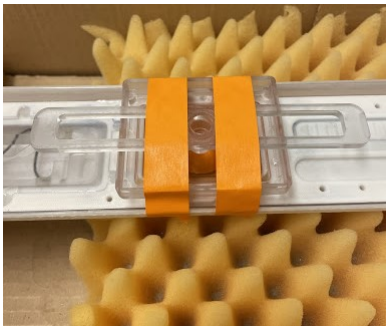

(b) Focal marker setup

Figure 2-7. Initial Setup and Focus Finding

Table 2-I. MRI parameters to for focal marker imaging

Parameter	Value
TE	2.1 ms
TR	120 ms
Number of Slices	15
Slice Thickness	1 mm
Frequency Encode Direction	S/I
Phase Encode Direction	AP
Slice Gap	0
Field of View	$60mm \times 60mm$
Acquisition Matrix	200×200

The coronal volume scans (2dseq file) were loaded into the RK-300 software. The orientation of the MRI with respect to the image was read-in from the metadata, and therefore, already accounted for in the software.

Using the interactive UI, the center of the cylinder (the focus) was set as the origin. To do that:

- With the cursor over the MRI volume image set, we scrolled to navigate through the slices.
- The green box was the limit of motor travel, and the blue square was the position where the focus was currently targeting (Figure 2-8).

- When the cursor was moved over the MRI slice image, a red crosshair at the tip of the cursor was observed.
- The center of the cylinder was targeted. When the cursor was at the center of the cylinder, a left-click was made.
- The red crosshairs were converted to a blue dot and a surrounding circle.

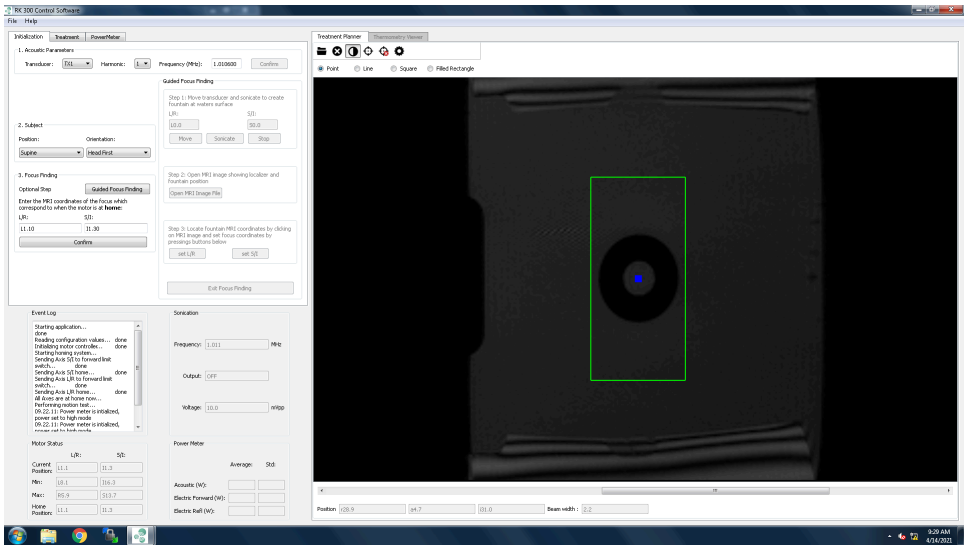

Figure 2-8. Loaded MRI scan to register the focus

Under "Step 3" of the "Guided Focus Finding", the "Set L/R" and "Set S/I" options were selected. The L/R and S/I coordinates were observed to update on the left, under "Focus Finding". The focus finding was then exited. Under "Focus Finding", with the newly updated values of L/R and S/I, the "Confirm" option was selected. On the right, the dark blue dot shifted to these coordinates (Figure 2-8). The system (focus) was thus registered with the MRI coordinates, and ready to use.

Sonication in a solid water phantom

After registering the focus, the RK-300 arm was slid out of the magnet. The focal marker and some water from the bath were removed. A solid water phantom from CIRS Inc. was placed in the bath, and taped down (Figure 2-9).

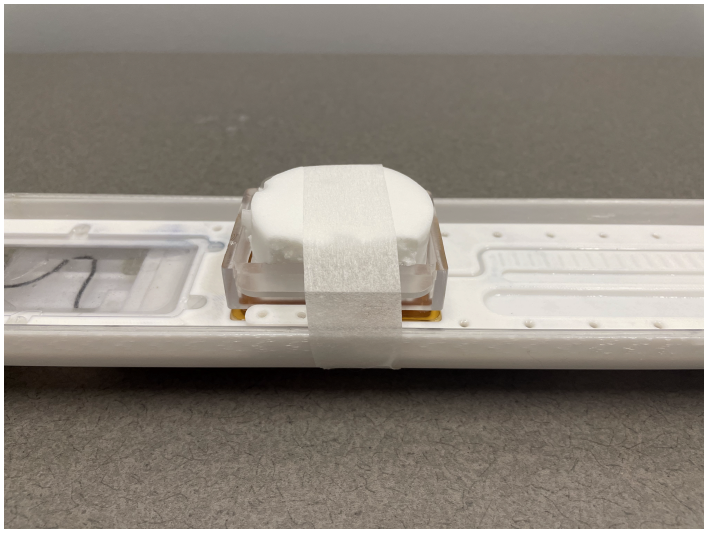

Figure 2-9. Solid-water phantom setup on the RK-300

This setup was then slid back into the bore of the MRI such that the center of the phantom was, again, at the isocenter of the magnet. Three-plane localizer images were acquired to ensure optimal positioning and the absence of air bubbles in the coupling medium. Coronal and axial T1w FLASH scans were then acquired. The parameters of the scan are provided in Table 2-II.

Table 2-II. MRI parameters for phantom imaging

Parameter	Value
TE	2.1 ms
TR	128 ms
Number of Slices	15
Slice Thickness	1 mm
Slice Gap	0
Field of View	$60mm \times 60mm$
Acquisition Matrix	200×200
Number of averages	4

The T1w axial scans were loaded into the RK-300 software. By scrolling through the slices, the axial slice that had the central cross-section of the transducer was selected. When the cursor is moved to different points in the image, the coordinates

corresponding to the cursor tip are reflected under the image. The cursor was moved to the lip of the transducer below the plastic holder, and the vertical coordinate was recorded. The focus of this transducer is geometrically fixed at 15.61mm. This value was subtracted from the vertical coordinate to get the focal plane.

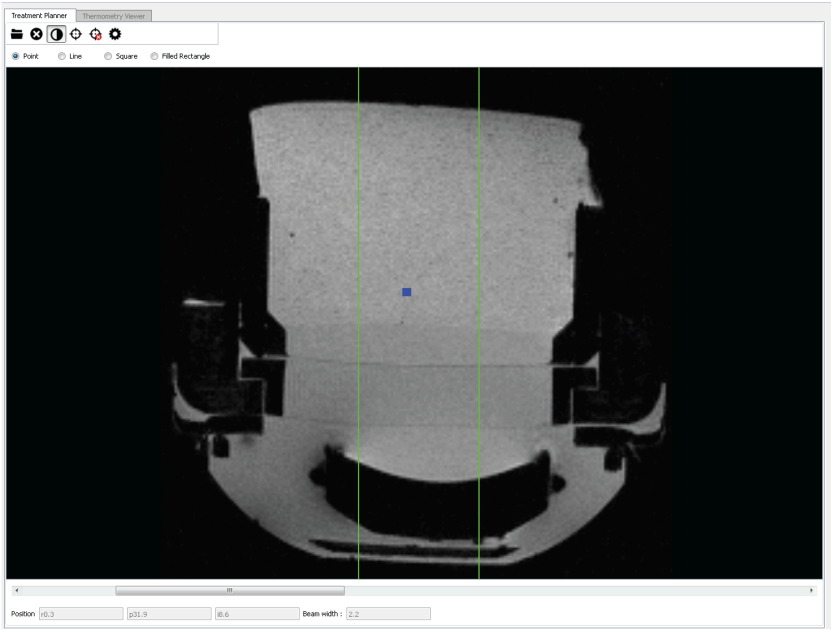

Figure 2-10. Treatment Planning: Axial View

The coronal scans were then loaded into RK-300 software. The slice corresponding to the vertical coordinate of the focal plane was selected. This was the plane in which we could target the focus of the ultrasound.

After selecting the single crosshairs tool under the "Treatment Planner" tab, the cursor was moved to a desired target, and with a left click, the target was selected. On the left, under the "Treatment" tab, the coordinates of the target appeared in the table (Figure 2-11).

In the Treatment tab, the row with the target coordinates was first selected and then "Go to Selected Target" was used to move the blue focal point to the red cross hair (desired point). The motor moved the transducer such that focus was now at the target point. This was verified by checking the status of the motors at the bottom

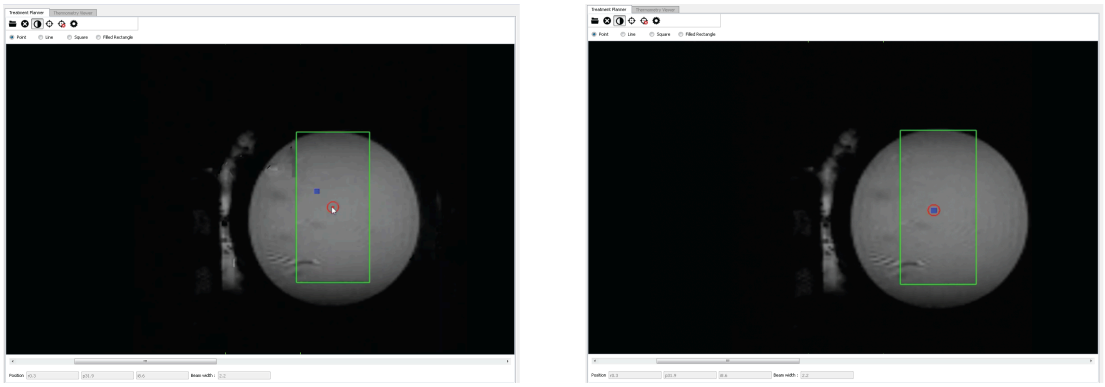

(a) Selecting the target **(b)** Confirming the target

Figure 2-11. Treatment Planning: Coronal View

of the tab. The horizontal plane coordinates of the transducer was the same as the target coordinates.

To sonicate, the "Continuous Wave" mode on the "Treatment" tab was selected, the "Power" was set to 2 Watts, sonication time to 15 seconds and wait time to 10 seconds. Single plane T1w FLASH axial scans were then acquired with the plane positioned at the S/I coordinate. The parameters of the scan are provided in Table 2-III. A total of 15 scans were acquired - 2 before sonication, and the rest during and after sonication. The scans put together (in post-processing) and showed a time sequence of the focus forming at the target.

Table 2-III. MRI parameters to observe sonication

Parameter	Value
TE	20 ms
TR	39 ms
Slice Thickness	1 mm
Field of View	$70mm \times 70mm$
Acquisition Matrix	128×128
Frequency Encode Direction	AP
Number of Averages	1
Flip Angle	20 degree
In plane dimensions (in plane resolution)	0.54×0.54

Results and Discussion

During sonication, that is, the delivery of the acoustic energy to the focus, a hyper-intense cone was seen from the surface of the transducer to the targeted focus (Figure 2-13). This hyper-intense region was a result of molecules in the medium vibrating under the influence of ultrasound. This was absent in the baseline scans acquired just before sonication (Figure 2-12).

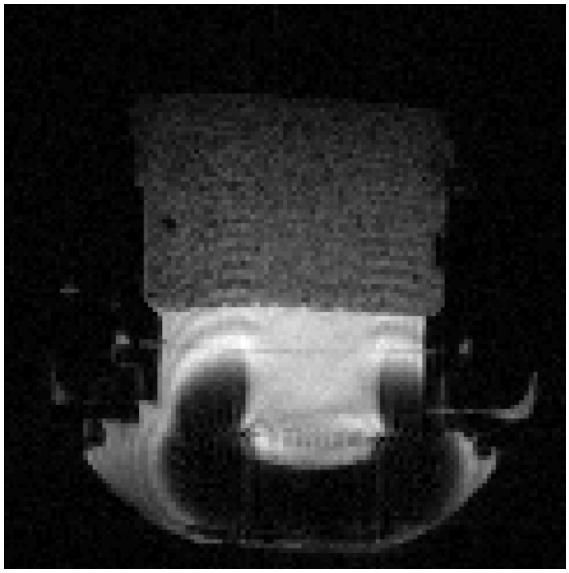

Figure 2-12. Pre-Sonication

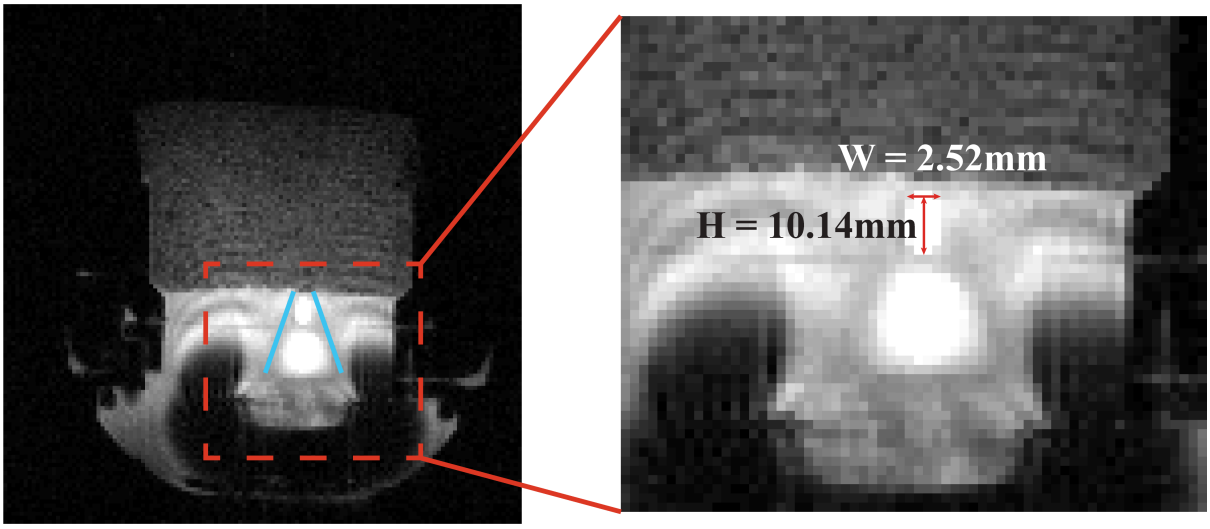

Figure 2-13. During Sonication (hyper-intense cone marked in blue)

Initially, an attempt was made to couple the phantom directly on the membrane cuboid using degassed ultrasound gel, but air bubbles got trapped as the gel folded over itself during application. Despite all attempts, an air bubble-free coupling was not achieved. Since the absence of air bubbles was crucial to observe focus formation, the phantom was immersed in the water bath which was then coupled to the membrane cuboid. This caused bubble-free coupling from the transducer to the phantom. However, it elevated the location of the phantom, such that, the geometrically fixed focus was formed near the outer surface of the phantom, and not well inside it. This was confirmed by the short axis and long-axis length of the tip of the cone formed.

Conclusion

The RK-300 at the Department of Radiology was seen to successfully target a location in a phantom, as observed by the single slice T1-weighted FLASH Time Sequence Images. By observing this targeting, the RK-300 can be utilized to perform a host of preclinical studies using different focused ultrasound applications.

This test can be used in Quality Control to ensure that the system is functioning as intended. It can also be used as a standard operating procedure for first-time users of the system.

Future Directions

Now that the RK-300 has been shown to successfully target a location inside a phantom, its ability to target in vivo models can be validated. A simple experiment to ensure correct targeting would be opening the BBB in a healthy rat (or mouse). Successful targeting can be observed using T1-weighted images with Gadolinium enhancement post treatment. The location at which the BBB is opened will be

observed as a hyper-intense region (due to the uptake of gadolinium at the site). This hyper-intense region can be cross-checked with the region targeted during treatment planning. An overlap of these two regions will indicate successful targeting.

After correct targeting in an animal is achieved, the RK-300 can be used to conduct any focused ultrasound application, with the exception of histotripsy (since the transducer and driving electronics were not designed to provide the high voltages required for histotripsy). A study to use the RK-300 to perform sonodynamic therapy in a U251 glioblastoma rat model is currently underway.

Chapter 3

Development of a Sensing System to Monitor CSF Pressure

The application of transcranial focused ultrasound involves delivering energy at a location inside the brain for a considerable duration of time. Therefore, care must be taken to ensure that this application of energy does not cause any detrimental downstream effects, one of which would be a deleterious increase in cerebrospinal fluid pressure.

Cerebrospinal Fluid (CSF) is a liquid that surrounds and circulates throughout the brain and spinal cord. It is responsible for not only cushioning the brain and spinal cord, but also delivering nutrients, chemicals, and oxygen while removing waste [59]. An increase in CSF pressure in the brain is regarded as a medical emergency because if left untreated, it can cause brain injury, stroke, coma, and death [60]. Therefore, monitoring this pressure during therapies to the brain is crucial.

Here, we look at the development of a sensing system that can be used to monitor CSF pressure in the brain (intracranial pressure). This system can be used to monitor intracranial pressure before, during, and after focused ultrasound treatments in the brain. By ensuring that CSF pressure does not dramatically change during or after focused ultrasound treatment, the associated severe effects can be avoided, and therefore, the safety of the treatment is assured.

Selection of Pressure Sensors

A pressure sensor consists of a transducer that can read the pressure of the medium in which it is placed in, convert it into electrical signals, and then interpret these signals as a numeric value. The composition of this transducer, and the principle it uses to read the pressure varies. There are many pressure sensors available, such as potentiometric, inductive, capacitive, piezo-based (piezoresistive and piezoelectric), reluctance, and fiber optics-based pressure sensors [61]. The two most common pressure sensors used in medicine are piezo-based pressure sensors and fiber optics-based pressure sensors.

Piezo-based Pressure Sensors

Piezo-elements are materials whose electrical properties change when force is applied to them. These can be further classified as piezoresistive and piezoelectric elements.

In a piezoresistive element (also known as a strain gauge) experiences a change in resistance when subjected to an applied force [62]. Therefore, if these materials are arranged in a Wheatstone Bridge configuration, as seen in Figure 3-1, the change in resistance corresponds to a change in the output voltage across the Bridge. Therefore, pressure can be measured as a function of voltage. Piezoresistive elements are commonly made up of germanium, polycrystalline silicon, amorphous silicon, silicon carbide, or single crystal silicon [63].

A piezoelectric element (such as quartz, PZT or PMNPT), is a material that generates a voltage when it experiences stress (as a result of pressure applied) [64]. This generated voltage is transient in nature, and is only generated during a change in the applied stress [65]. The advantage of this element is that it acts as a voltage source (which is a function of pressure), and therefore, does not require a voltage source setup for measuring pressure. The disadvantage, however, is that it cannot

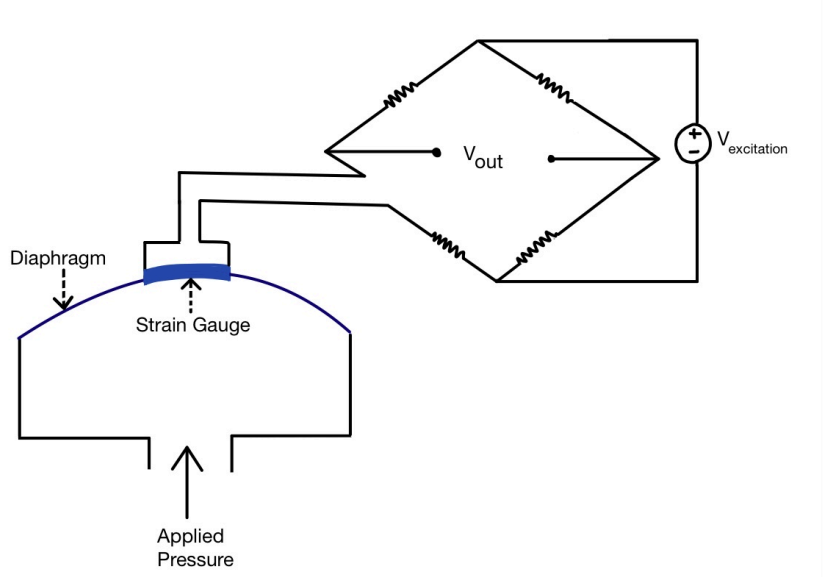

Figure 3-1. The strain gauge is attached to a diaphragm. When the diaphragm deflects, as a result of pressure, the resistance of the strain gauge changes

be used to continuously measure a constant pressure, but rather can only measure changes in pressure.

Management of intracranial pressure measurement requires continuous measurements of varying pressure and constant pressure, leading to piezo-resistive elements being commonly used

There are three broad methods of placing the piezo-resistive sensor to measure intracranial pressure:

- In the brain parenchyma
- Between the brain parenchyma and dura
- In the ventricles

These sensors are accurate, but their readings drift from the true value due to their sensitivity to temperature [66, 67]. They also have a relatively larger form factor (sensor size) for higher pressure sensitivity and lower power requirements [68]. However, these shortcomings are not exhibited by fiber optics-based pressure sensors.

Fiber Optics-based Pressure Sensors

General Principle of Fiber Optics:

Light is an electromagnetic wave that consists of an electric and magnetic field traveling mutually perpendicular to each other (Figure 3-2). Therefore, light can be treated as a ray - a straight line with both magnitude and direction.

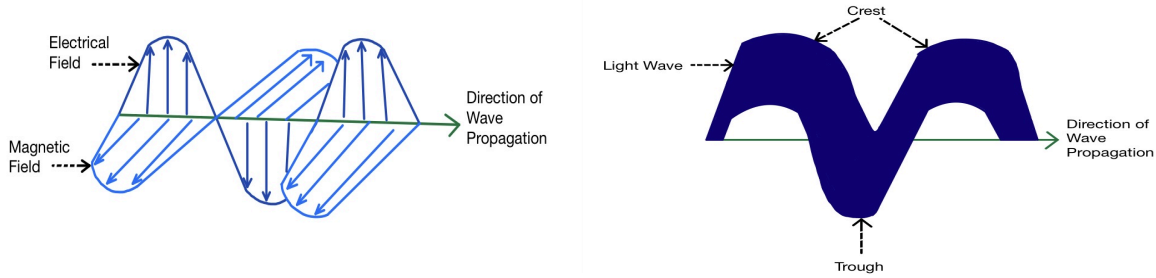

(a) Mutually perpendicular electric and magnetic fields

(b) Resulting light wave

Figure 3-2. Light as an electromagnetic wave

When light travels from an optically denser to rarer medium, it bends away from the normal (dark blue vector in Figure 3-3.a), that is, a perpendicular drawn at the interface of the surface. As the angle of the light in the denser medium increases, the corresponding angle in the rarer medium increases, till at one point, light in the rarer medium travels along the denser-rarer medium interface (neon-green vector in Figure 3-3.a). The corresponding angle in the denser medium is called the critical angle (θ_c in Figure 3-3.a). When light is incident at a denser-rarer medium at an angle greater than the critical angle, it is completely reflected back into the denser medium (red vector in Figure 3-3.a). This principle is known as total internal reflection and is used to propagate light in a fiber optic cable [69].

A fiber optic cable has a core and cladding. The core is made up of a material with optical density greater (higher refractive index) than that of the cladding. Therefore, if light enters the fiber in a suitable fashion, it will keep hitting the core-cladding

interface at an angle greater than the critical angle. Therefore, light will bounce off the walls of the fiber, as it propagates along the fiber [69] (Figure 3-3 (b)).

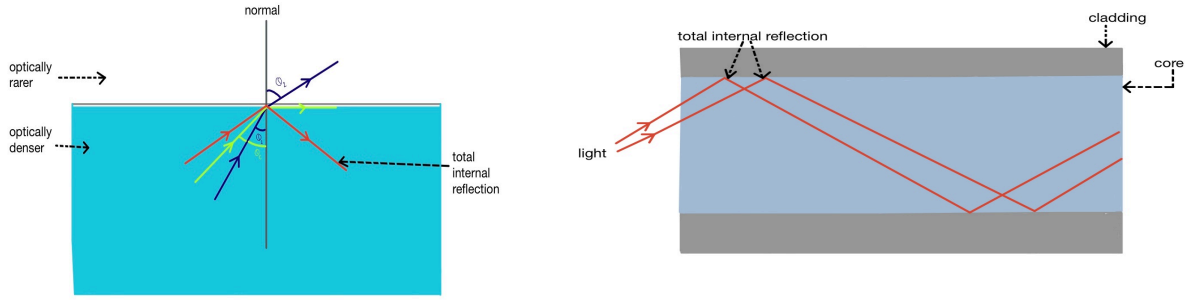

(a) Total internal reflection **(b)** Light propagation in a fiber

Figure 3-3. Total internal reflection and light propagating along a fiber optic

In addition to the cable, fiber optic sensor system is made up of a sensor and a signal conditioner. The signal conditioner consists of a light source, and a detector. The light source sends light to the sensor through the fiber optic cable, the light interacts in the sensor, and the detector interprets the light reflected back from the sensor. The sensor that lies on the tip of the fiber varies based on the physical phenomenon being measured. Pressure is measured using the Fabry-Pérot Cavity.

Fabry-Pérot Cavity

The Fabry-Pérot Cavity can be used to measure the pressure of the medium in which it is placed. As seen in Figure 3-4, the sensor is made up of a vacuum chamber and two partially reflective surfaces on either side. The outer surface is a partially reflective diaphragm (flexible membrane) while the inner surface is fixed. Light from the source propagates through the fiber and is first incident on the inner surface. Some light is partially reflected off that surface back to the detector, and the rest of the light is in turn reflected from the diaphragm. The reflected light beams from both the surfaces have a phase difference, which causes an interference pattern on the detector (in this case an interferometer). In response to the environment's pressure, the

diaphragm deflects, and the distance between the two surfaces changes. Therefore, the interference pattern changes. The initial distance is calibrated to a particular baseline pressure, and subsequent changes in distance correspond to changes in pressure from this baseline [70].

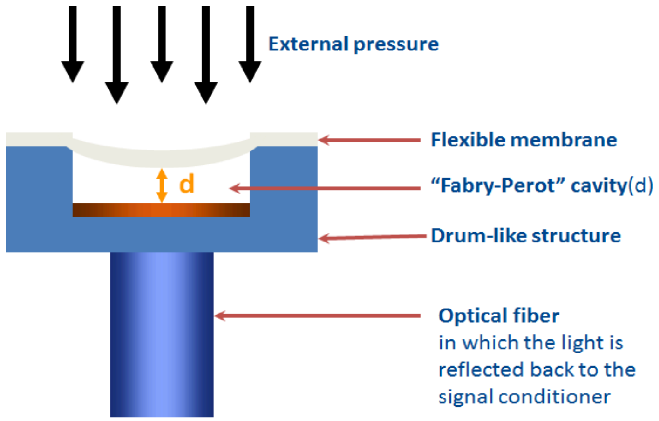

Figure 3-4. Fiber tip comprising the Fabry-Pérot Cavity (reproduced with permission from [70])

Since the Fabry-Pérot based Fiber Optic Sensor has a smaller form factor (size) than piezo-resistive sensors, it is an interesting option to explore for measuring intracranial pressure for prolonged durations of time.

FOP-M260 by FISO

The FOP-M260 sensor by FISO is a Fabry-Pérot based Fiber Optic Sensor used to measure pressure [70]. It is conventionally placed in a catheter which is inserted into the target region in the body where pressure needs to be monitored. It consists of a fiber optic cable with the Fabry-Pérot Cavity at the tip of the cable (Figure 3-5). A polyimide tubing encloses the fiber optic. This tubing conventionally covers the entire cable including the sensor tip. After the fiber optic has been successfully threaded into the catheter, the polyimide tubing can be pulled back to expose the sensor tip. Therefore, the polyimide tubing serves as protection to the sensor and fiber optic cable.

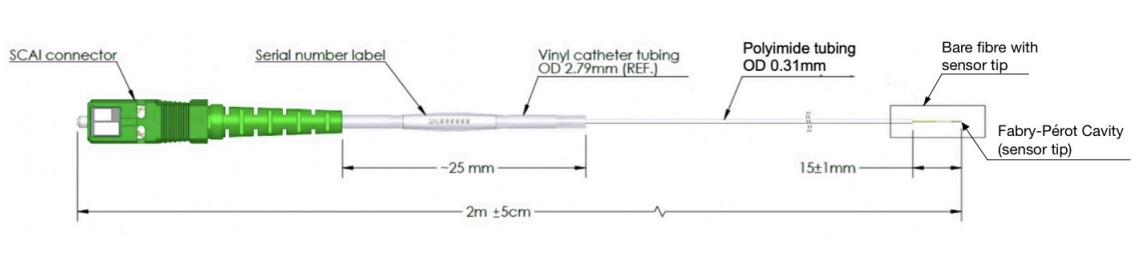

Figure 3-5. FOP-M260 Sensor Schematic (reproduced with permission from [70])

The fiber optic cable is connected to the signal conditioning module using a SCAI connector. As previously mentioned, the signal conditioner houses the light source and the interferometer. The signal conditioner can be connected to a laptop using a USB connector. The Evolution software by FISO, installed on a laptop, serves as the processor and user interface. It can be used to calibrate the sensor (the FOP-M260 was calibrated by the manufacturer using a polynomial regression algorithm, where $Pressure = 14.52103 - 0.01429 * (internal_reading - center)^1 + 2.67E-06 * (internal_reading - center)^2 - 1.93E-09 * (internal_reading - center)^3$) , set atmospheric pressure to zero, and read out values from the signal conditioner. The pressure value recorded can be stored and used for data analysis.

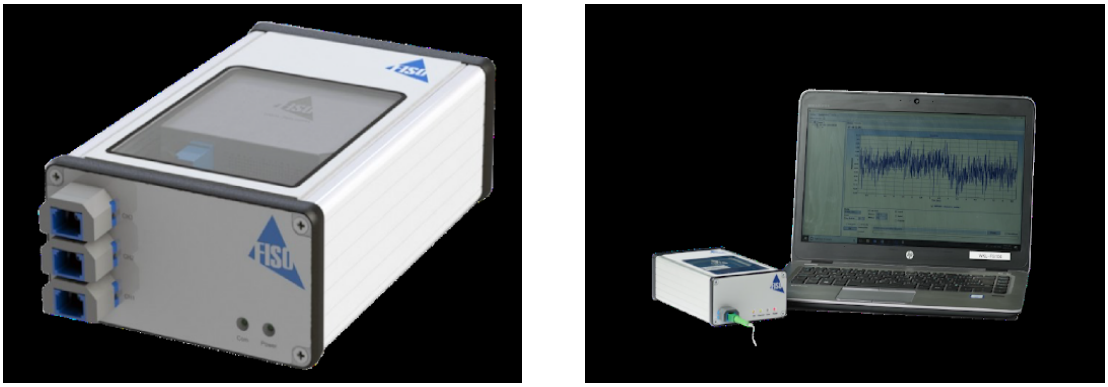

(a) FISO Pressure Signal Conditioning Module **(b)** FISO Pressure Sensing Configuration

Figure 3-6. FISO pressure sensing module and user interface (reproduced with permission from [70])

The parameters as listed in Table 3-1 make it suitable for measuring intracranial pressure, and is therefore the sensor we will be testing with the end-goal of using it to measure intracranial pressure.

Table 3-I. Specifications of the FOP-M260 by FISO

Parameter	Value
Outer Diameter (sensor tip)	0.26 mm
Outer Diameter (with polyimide tubing)	0.31 mm
Bare Fiber Length	2 m
Polyimide Tube Length	2 m
Pressure Range (relative to atmospheric pressure)	-300 mmHg to +300 mmHg
Resolution	< 0.3 mm of Hg
Operating Temperature Range	15°C to 45°C
Long Term Bending Radius (Minimum)	17 mm
Sterilization Method	Ethylene oxide sterilization (EtO)
Sampling Frequency	250 Hz
Epoxy Coating	Yes, just not on sensor tip
Used in medical applications	Yes

System Requirements

The testing to be conducted on the pressure sensor was driven by the requirements outlined in Table 3-II. The performance requirements were determined by existing standards for pressure sensors, and discussions with clinical experts. Table 3-II provides an overview of the sensor requirements and the test to be conducted to verify the requirements. The following sections will describe the testing procedures in greater depth and the results of the testing.

Table 3-II. System Requirements

Number	Type	Description	Testing Method
1	Performance	The sensor shall be able to maintain pressure readings within the specified resolution for up to hours	Drift testing
2	Performance	The sensor shall be able to maintain pressure readings within the specified resolution as temperature changes between 35-39 ^{o}C	Temperature Stability of Measurement
3	Design	The sensor shall maintain readings with the specified resolution while experiencing a bend radius of 17 mm	Bend Radius testing
4	Performance	Overall Sensor Range shall be between 1 to 40 mmHg with a resolution $\leq 1mmHg$	Accuracy testing

Experimental Design

Initial testing was carried out to ensure that the acquired COTS (commercially available off-the-shelf components) sensor met the system requirements. For this testing, a hydrostatic water column setup was utilized. Pressure was be determined by water increments in the column and can be calculated by the equation below.

$$P = \rho \times h \times g$$

Where, P = pressure (pascal); ρ = density of water, which is $999.9kg/m^3$; h = height in the water column (in meters); g = acceleration due to gravity, which is $9.8m/s^2$

$$P = 999.9 \times h \times 10^{-2} \times 9.8$$

$$P = (97.99 \times h)Pascals$$

$$P = \frac{97.99h}{133.32}mmHg = (0.7h)mmHg$$

The image below (Figure 3-7) highlights the experimental setup used for the preliminary testing. A 4000 ml hydrostatic column was used. This allowed for absolute pressures (not relative to the atmospheric pressure) from 0 mmHg to 40 mmHg. The

fiber optic was fixed such that the sensor tip was close to the bottom of this column. Then the pressure was varied by varying the height of the column while leaving the sensor in place. The main aim of the tests conducted was to verify the optical fiber sensor when tested met specified requirements and manufacturer specifications. The tests described are influenced by the ANSI/AAMI NS28:1988/(R)2010 for Intracranial pressure monitoring devices.

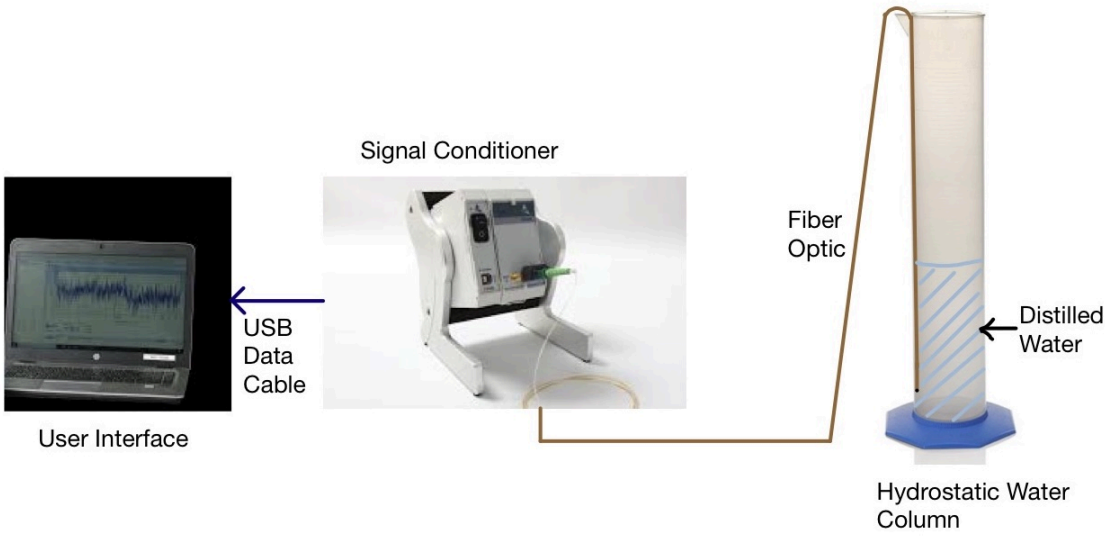

Figure 3-7. ACMI Test-Bench Setup

Drift Test

Zero drift testing for pressure sensors help us understand if zero drift occurs in the beginning during the settling period or if long term use causes deterioration of functionality. For this test, the sensor was left in the box in which it came. This served as a simple method to hold the sensor in place. The polyimide tubing was slid back to expose the sensor (the sensor is generally covered by the polyimide tubing to protect it). The lid of the box was placed over the sensor except for some room to allow the proximal end of the fiber optic to connect to the signal conditioner sitting

outside the box. The pressure of the sensor inside the box was recorded at a sampling frequency of 250 Hz for 24 hours. The recorded pressure was then passed through a low pass filter with a cutoff frequency of 1 Hz (since static pressure is being measured) and then plotted as a function of time.

Temperature Stability of Measurement

This test aims to evaluate the performance of the pressure sensor under varying temperature conditions. The column was filled up such that the height of the water column above the sensor was 10 cm. In this test, the water used to fill the hydrostatic column was about 42°C. This temperature was confirmed used a negative temperature coefficient thermistor-based temperature sensor. This temperature sensor was then placed inside the hydrostatic column to monitor temperature. The pressure was then recorded as the temperature naturally cooled down to a temperature of 27°C. This test was repeated for a water column height of 19 cm. The pressure reading was expected to stay constant as temperature varied.

Accuracy Test

For this testing, a hydrostatic column was used. Using the hydrostatic column allows for the pressure exerted by the column to be calculated (as discussed above). These calculations serve as a 'reliable' reference sensor.

The pressure of the hydrostatic column was varied from 2 cm to 40 cm inches in 2 cm increments. The pressure at each level was recorded by the pressure sensor for 5 minutes in triplicates. The pressure difference between each successive pressure recorded was then calculated. The pressure difference between each successive reading should be 1.4711 mmHg. This difference was used to verify accuracy of the system.

Bend Radius Testing

To position the pressure sensor, it is placed in a catheter, and the catheter is threaded to the target location. As the catheter is threaded to the target location, it is often bent. With fiber optics, bending the fiber optic such that its bending radius is less than the minimum bending radius for the core-cladding combination risks breaking the fiber as well as affecting the light path to and from the sensor tip, and therefore, affect the pressure reading. The effects of exceeding the minimum bending radius include:

- Higher attenuation
- Damage to the cable structure
- Possibility of breaking the fiber

The FOP-M260 by FISO has a manufacturer recommended minimum long-term bending radius (the minimum radius the fiber can be deformed to prolonged periods) of 17 mm.

The pressure in the column was maintained at a water column height of 34 cm above the sensor. The fiber was then looped such that it was 30 mm, 17mm, and 8.5 mm (in three separate cases), and the pressure was recorded for 1 hour.

Results and Discussion

Zero Drift Test Results

The sensor showed no significant variation (drift) over 20 hours with a slight decrease (about 3 mmHg) in the last four hours of recording (Figure 3-8). This dip in pressure towards the end could have been a result of changing weather conditions, since the pressure sensor can pick up even the slightest change in pressure.

The pressure sensor readings did not drift significantly. However, the slight decrease in pressure towards the end of the test period needs to be further investigated. This can be done by repeated testing, or testing zero drift in a hydrostatic column to minimize the effect of changes in atmospheric pressure).

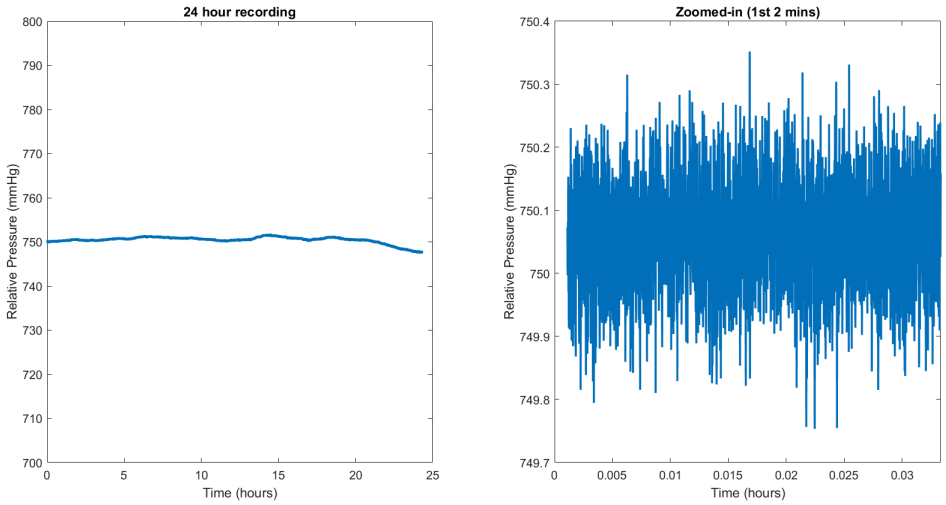

Figure 3-8. Pressure Sensor Zero Drift Test Results

Temperature Stability of Measurement Test Results

As seen in Figure 3-9, the pressure decreased by about 4mmHg (in both the cases) during the first 30 seconds and remained constant for the remaining duration of the test. Therefore, the stability of measurement results met our system requirements with pressure not varying significantly as temperature of the water column it was placed in varied.

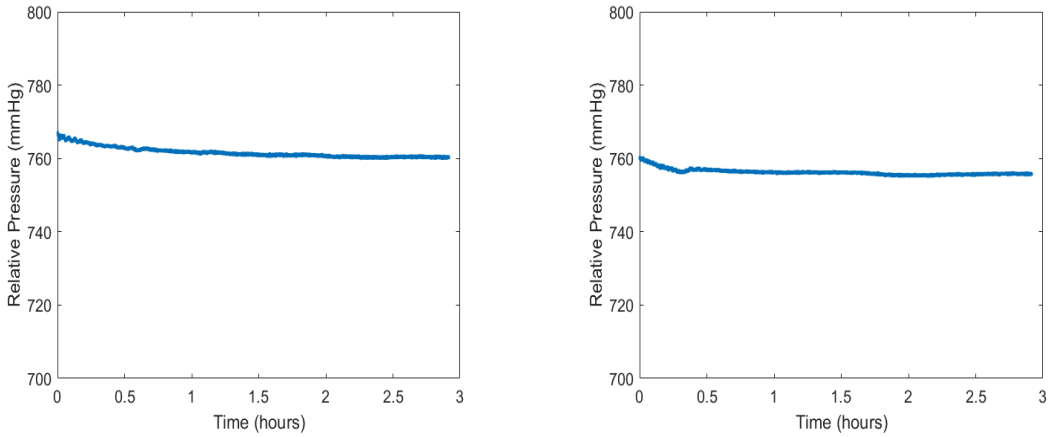

(a) Relative Pressure at 19 cm **(b)** Relative Pressure at 10 cm

Figure 3-9. Stability of measurement tests results

Accuracy Test Results

For accuracy of the system, since the pressure sensor measured pressure relative to atmospheric pressure, a change in pressure between successive readings was used to verify accuracy of the pressure recorded by the sensor.

In Figure 3-10, the blue line graph shows the increase in pressure with increase in height of the water column. The black error bars correspond to the deviation of changes in pressure from 1.4711 mmHg. The numeric values of these errors are provided in Table 3-III. Since 2 cm was the first value recorded, the recorded pressure difference from a previous value cannot be calculated, and therefore, its recorded error is assumed to be zero.

The average error calculated was 0.227 mmHg. This met the accuracy requirements for our application. The largest error was recorded at 6cm with a 1.11 mmHg difference. This was not a concern since variation was expected based on how the test was conducted, that is, the height of the water column was measured manually.

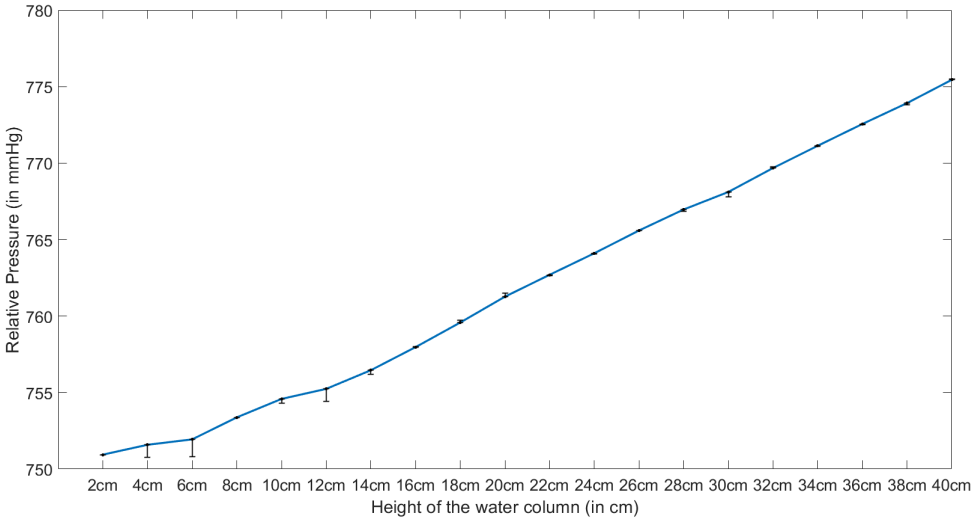

Figure 3-10. Pressure Sensor Accuracy Test Results

Table 3-III. Pressure Sensor Accuracy Testing

Water column height (cm)	Measured Difference (mmHg)
2	0
2 - 4	-0.8256
4 - 6	-1.1168
6 - 8	-0.0333
8 - 10	-0.2652
10 - 12	-0.8149
12 - 14	-0.2502
14 - 16	0.0370
16 - 18	0.1370
18 - 20	0.2177
20 - 22	-0.0392
22 - 24	-0.0650
24 - 26	0.0157
26 - 28	-0.0979
28 - 30	-0.3242
30 - 32	0.0926
32 - 34	-0.0168
34 - 36	-0.0466
36 - 38	-0.1041
36 - 40	0.0486

Bend Radius Test Results

The sensor performed as per manufacture specifications when the bend radius of the fiber optic was held at 17mm and 30mm, respectively. Despite the manufacturer recommending that the bend radius of the fiber not be held under 17 mm, the recorded pressure value varied from the above values by 1 mmHg when the bend radius of the fiber was held at 8.5 mm during data acquisition (Figure 3-11).

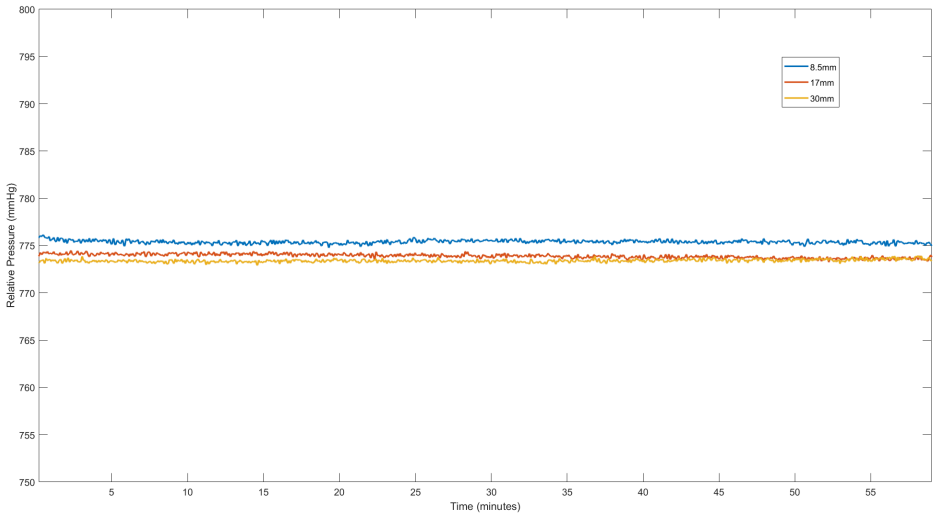

Figure 3-11. Bend Radius Test Results

Conclusion

By passing the preliminary round of testing, the Fabry-Pérot - based Fiber Optic Pressure Sensor by FISO (FOP-M260) shows potential to be used in measuring pressure accurately and reliably.

Future Directions

After successful bench-top testing, the immediate step would be to replace the hydrostatic column with a pulsed pressure generator regulated system, and repeat all the tests conducted above. This is because the intracranial pressure is pulsatile, and the pressure sensor should be able to maintain its performance while reading pulsating pressure.

Chapter 4

Conclusions and General Discussions

Focused ultrasound is ushering in an exciting era of non-invasive and effective treatments for brain diseases. The literature reflects this increase in research in the field with great promise of translatable treatments. Thermal ablation to treat essential tremor has been FDA approved, along with opening the BBB for drug delivery in the treatment of Parkinson's disease. In addition to these approved treatments, the FDA has approved BBB opening to treat brain tumors and Alzheimer's disease. These approved treatments and clinical treatments are only the beginning for translatable applications.

All these clinical trials are built on the foundation of rigorous animal studies. The RK-300 by FUS Instruments has proven to be vital in different focused application studies in small animals. It is versatile in the applications of focused ultrasound it can support. It has been instrumental in studies using focused ultrasound to perform thermal ablation, BBB opening for drug delivery, and sonodynamic therapy. The system cannot be used to observe histotripsy in the treatment of brain tumors because the transducer and driving electronics cannot support the high voltages that are necessary to produce the high peak pressure in vivo. However, the applications the system can perform, makes it a vital tool in preclinical studies.

Safety in these treatments is important - these treatments should not cause any downstream effects. In applications of focused ultrasound in the brain, the cerebrospinal fluid is an important parameter that should be monitored especially as focused ultrasound establishes itself as a form of therapy. The Fabry-Pérot Cavity - based pressure sensor by FISO shows great promise in being used as a minimally-invasive method to measure intracranial pressure. The fiber optic system tested here was demonstrated to meet all the manufacturer's standards. Additionally, by successfully passing the zero-drift, accuracy, bend radius, and stability of measurement test, the FOP-M260 by FISO is an excellent candidate to measure intracranial pressure before, during, and after focused ultrasound-based treatments.

Where is Focused Ultrasound heading?

Focused ultrasound is progressing, especially for treating brain diseases. It is already utilized for the treatment of essential tremor and Parkinson's Disease. In the near future, we will see it being used in the treatment of brain tumors (using histotripsy, blood-brain barrier opening - aided chemotherapy), and Alzheimer's Disease.

Preclinical studies form the backbone of translation. There is a lot of research on designing and improving the instruments used for pre-clinical studies. For example, when it comes to the RK-300, work is being done to better integrate the RK-300 with the MRI system. The version of the RK-300 that was used for the phantom test is an earlier version of the software that is currently sold with the system. While using the earlier version of the software, the RK-300 has to be slid in and out of the MRI twice - once to register the focus of the system and the second time, to carry out the treatment. When the RK-300 is slid back into the magnet for treatment, if it is not placed at the same position in the magnet as before, an error is introduced, and this error will affect the coordinates of the desired focus target(s). The new version of the software that is sold with the system eliminates the need to slide the arm out of the RK-300 for a particular animal study, therefore, allowing for better accuracy in focus targeting.

Concerning potential measurement of intracranial pressure, as mentioned earlier, the Fabry-Pérot Cavity-based pressure sensor by FISO shows great promise. The

successful preliminary testing has set the stage for more rigorous testing for translation to the clinic. Since intracranial pressure is pulsatile, the tests performed (with the exception of the zero drift test), need to be performed with pulsatile pressure. This can be done by swapping out the hydrostatic column with a closed system where a pulsed pressure generator regulates the pressure. After this has been successfully performed, progress can be made to small animal studies followed by larger animal studies and then clinical trials.

In conclusion, research in the field of focused ultrasound is progressing at a rapid pace. With surgeons and engineers working together, it will not be long before focused ultrasound is treated as a "conventional" therapy or maybe even in the "gold standard" in treating certain diseases.

References

[1] A. Carovac, F. Smajlovic, and D. Junuzovic, "Application of ultrasound in medicine," *Acta Inform Med*, vol. 19, no. 3, pp. 168–71, 2011. [Online]. Available: https://www.ncbi.nlm.nih.gov/pubmed/23408755

[2] T. R. Nelson, J. B. Fowlkes, J. S. Abramowicz, and C. C. Church, "Ultrasound biosafety considerations for the practicing sonographer and sonologist," *J Ultrasound Med*, vol. 28, no. 2, pp. 139–50, 2009. [Online]. Available: https://www.ncbi.nlm.nih.gov/pubmed/19168764

[3] C. Lafon, D. Melodelima, R. Salomir, and J. Y. Chapelon, "Interstitial devices for minimally invasive thermal ablation by high-intensity ultrasound," *Int J Hyperthermia*, vol. 23, no. 2, pp. 153–63, 2007. [Online]. Available: https://www.ncbi.nlm.nih.gov/pubmed/17578339

[4] D. S. Hersh, A. J. Kim, J. A. Winkles, H. M. Eisenberg, G. F. Woodworth, and V. Frenkel, "Emerging applications of therapeutic ultrasound in neuro-oncology: Moving beyond tumor ablation," *Neurosurgery*, vol. 79, no. 5, pp. 643–654, 2016. [Online]. Available: https://www.ncbi.nlm.nih.gov/pubmed/27552589

[5] R. Daneman and A. Prat, "The blood-brain barrier," *Cold Spring Harb Perspect Biol*, vol. 7, no. 1, p. a020412, 2015. [Online]. Available: https://www.ncbi.nlm.nih.gov/pubmed/25561720

[6] K. K. Jain, "Nanobiotechnology-based drug delivery to the central nervous system," *Neurodegener Dis*, vol. 4, no. 4, pp. 287–91, 2007. [Online]. Available:

https://www.ncbi.nlm.nih.gov/pubmed/17627131

[7] S. J. Madsen and H. Hirschberg, "Site-specific opening of the blood-brain barrier," *J Biophotonics*, vol. 3, no. 5-6, pp. 356–67, 2010. [Online]. Available: https://www.ncbi.nlm.nih.gov/pubmed/20162563

[8] S. I. Rapoport, "Osmotic opening of the blood-brain barrier," *Ciba Found Symp*, no. 56, pp. 237–55, 1978. [Online]. Available: https://www.ncbi.nlm.nih.gov/pubmed/97064

[9] E. E. Konofagou, Y. S. Tung, J. Choi, T. Deffieux, B. Baseri, and F. Vlachos, "Ultrasound-induced blood-brain barrier opening," *Curr Pharm Biotechnol*, vol. 13, no. 7, pp. 1332–45, 2012. [Online]. Available: https://www.ncbi.nlm.nih.gov/pubmed/22201586

[10] A. Burgess, K. Shah, O. Hough, and K. Hynynen, "Focused ultrasound-mediated drug delivery through the blood-brain barrier," *Expert Rev Neurother*, vol. 15, no. 5, pp. 477–91, 2015. [Online]. Available: https://www.ncbi.nlm.nih.gov/pubmed/25936845

[11] L. H. Treat, N. McDannold, N. Vykhodtseva, Y. Zhang, K. Tam, and K. Hynynen, "Targeted delivery of doxorubicin to the rat brain at therapeutic levels using mri-guided focused ultrasound," *Int J Cancer*, vol. 121, no. 4, pp. 901–7, 2007. [Online]. Available: https://www.ncbi.nlm.nih.gov/pubmed/17437269

[12] D. S. Hersh, A. S. Wadajkar, N. Roberts, J. G. Perez, N. P. Connolly, V. Frenkel, J. A. Winkles, G. F. Woodworth, and A. J. Kim, "Evolving drug delivery strategies to overcome the blood brain barrier," *Curr Pharm Des*, vol. 22, no. 9, pp. 1177–1193, 2016. [Online]. Available: https://www.ncbi.nlm.nih.gov/pubmed/26685681

[13] J. Le Floc'h, H. D. Lu, T. L. Lim, C. Démoré, R. K. Prud'homme, K. Hynynen, and F. S. Foster, "Transcranial photoacoustic detection of blood-brain

barrier disruption following focused ultrasound-mediated nanoparticle delivery," *Mol Imaging Biol*, vol. 22, no. 2, pp. 324–334, 2020. [Online]. Available: https://www.ncbi.nlm.nih.gov/pubmed/31286352

[14] R. M. Jones, L. Deng, K. Leung, D. McMahon, M. A. O'Reilly, and K. Hynynen, "Three-dimensional transcranial microbubble imaging for guiding volumetric ultrasound-mediated blood-brain barrier opening," *Theranostics*, vol. 8, no. 11, pp. 2909–2926, 2018. [Online]. Available: https://www.ncbi.nlm.nih.gov/pubmed/29896293

[15] Z. K. Englander, H. J. Wei, A. N. Pouliopoulos, E. Bendau, P. Upadhyayula, C. I. Jan, E. F. Spinazzi, N. Yoh, M. Tazhibi, N. M. McQuillan, T. J. C. Wang, J. N. Bruce, P. Canoll, N. A. Feldstein, S. Zacharoulis, E. E. Konofagou, and C. C. Wu, "Focused ultrasound mediated blood-brain barrier opening is safe and feasible in a murine pontine glioma model," *Sci Rep*, vol. 11, no. 1, p. 6521, 2021. [Online]. Available: https://www.ncbi.nlm.nih.gov/pubmed/33753753

[16] K. T. Chen, K. C. Wei, and H. L. Liu, "Theranostic strategy of focused ultrasound induced blood-brain barrier opening for cns disease treatment," *Front Pharmacol*, vol. 10, p. 86, 2019. [Online]. Available: https://www.ncbi.nlm.nih.gov/pubmed/30792657

[17] T. Mainprize, N. Lipsman, Y. Huang, Y. Meng, A. Bethune, S. Ironside, C. Heyn, R. Alkins, M. Trudeau, A. Sahgal, J. Perry, and K. Hynynen, "Blood-brain barrier opening in primary brain tumors with non-invasive mr-guided focused ultrasound: A clinical safety and feasibility study," *Sci Rep*, vol. 9, no. 1, p. 321, 2019. [Online]. Available: https://www.ncbi.nlm.nih.gov/pubmed/30674905

[18] C. Brace, "Thermal tumor ablation in clinical use," *IEEE Pulse*, vol. 2, no. 5, pp. 28–38, 2011. [Online]. Available: https://www.ncbi.nlm.nih.gov/pubmed/25372967

[19] T. J. Dubinsky, C. Cuevas, M. K. Dighe, O. Kolokythas, and J. H. Hwang, "High-intensity focused ultrasound: current potential and oncologic applications," *AJR Am J Roentgenol*, vol. 190, no. 1, pp. 191–9, 2008. [Online]. Available: https://www.ncbi.nlm.nih.gov/pubmed/18094311

[20] D. Coluccia, J. Fandino, L. Schwyzer, R. O'Gorman, L. Remonda, J. Anon, E. Martin, and B. Werner, "First noninvasive thermal ablation of a brain tumor with mr-guided focused ultrasound," *J Ther Ultrasound*, vol. 2, p. 17, 2014. [Online]. Available: https://www.ncbi.nlm.nih.gov/pubmed/25671132

[21] E. M. Lillie, J. E. Urban, A. A. Weaver, A. K. Powers, and J. D. Stitzel, "Estimation of skull table thickness with clinical ct and validation with microct," *J Anat*, vol. 226, no. 1, pp. 73–80, 2015. [Online]. Available: https://www.ncbi.nlm.nih.gov/pubmed/25441171

[22] F. J. Fry and J. E. Barger, "Acoustical properties of the human skull," *J Acoust Soc Am*, vol. 63, no. 5, pp. 1576–90, 1978. [Online]. Available: https://www.ncbi.nlm.nih.gov/pubmed/690336

[23] J. F. Aubry and M. Tanter, "Mr-guided transcranial focused ultrasound," *Adv Exp Med Biol*, vol. 880, pp. 97–111, 2016. [Online]. Available: https://www.ncbi.nlm.nih.gov/pubmed/26486334

[24] M. Belzberg, S. Mahapatra, A. Perdomo-Pantoja, F. Chavez, K. Morrison, K. T. Xiong, N. J. Gamo, S. Restaino, N. Thakor, Y. Yazdi, R. Iyer, B. Tyler, N. Theodore, M. G. Luciano, H. Brem, M. Groves, A. R. Cohen, and A. Manbachi, "Minimally invasive therapeutic ultrasound: Ultrasound-guided ultrasound ablation in neuro-oncology," *Ultrasonics*, vol. 108, p. 106210, 2020. [Online]. Available: https://www.ncbi.nlm.nih.gov/pubmed/32619834

[25] M. S. Canney, F. Chavrier, S. Tsysar, J. Y. Chapelon, C. Lafon, and A. Carpentier, "A multi-element interstitial ultrasound applicator for the thermal

therapy of brain tumors," *J Acoust Soc Am*, vol. 134, no. 2, pp. 1647–55, 2013. [Online]. Available: https://www.ncbi.nlm.nih.gov/pubmed/23927205

[26] Z. Hu, X. Y. Yang, Y. Liu, M. A. Morse, H. K. Lyerly, T. M. Clay, and P. Zhong, "Release of endogenous danger signals from hifu-treated tumor cells and their stimulatory effects on apcs," *Biochem Biophys Res Commun*, vol. 335, no. 1, pp. 124–31, 2005. [Online]. Available: https://www.ncbi.nlm.nih.gov/pubmed/16055092

[27] E. Vlaisavljevich, A. Maxwell, M. Warnez, E. Johnsen, C. A. Cain, and Z. Xu, "Histotripsy-induced cavitation cloud initiation thresholds in tissues of different mechanical properties," *IEEE Trans Ultrason Ferroelectr Freq Control*, vol. 61, no. 2, pp. 341–52, 2014. [Online]. Available: https://www.ncbi.nlm.nih.gov/pubmed/24474139

[28] Z. Xu, M. Raghavan, T. L. Hall, M. A. Mycek, and J. B. Fowlkes, "Evolution of bubble clouds induced by pulsed cavitational ultrasound therapy - histotripsy," *IEEE Trans Ultrason Ferroelectr Freq Control*, vol. 55, no. 5, pp. 1122–32, 2008. [Online]. Available: https://www.ncbi.nlm.nih.gov/pubmed/18519220

[29] Z. Xu, A. Ludomirsky, L. Y. Eun, T. L. Hall, B. C. Tran, J. B. Fowlkes, and C. A. Cain, "Controlled ultrasound tissue erosion," *IEEE Trans Ultrason Ferroelectr Freq Control*, vol. 51, no. 6, pp. 726–36, 2004. [Online]. Available: https://www.ncbi.nlm.nih.gov/pubmed/15244286

[30] "Histosonics initiates first liver tumor clinical trial in the us," https://www.fusfoundation.org/news/histosonics-initiates-first-liver-cancer-clinical-trial-in-the-us, note = Accessed: 2021-04-14.

[31] E. Vlaisavljevich, Y. Y. Durmaz, A. Maxwell, M. Elsayed, and Z. Xu, "Nanodroplet-mediated histotripsy for image-guided targeted ultrasound cell

ablation," *Theranostics*, vol. 3, no. 11, pp. 851–64, 2013. [Online]. Available: https://www.ncbi.nlm.nih.gov/pubmed/24312155

[32] J. Sukovich, Z. Xu, Y. Kim, H. Cao, T. S. Nguyen, A. Pandey, T. Hall, and C. Cain, "Targeted lesion generation through the skull without aberration correction using histotripsy," *IEEE Trans Ultrason Ferroelectr Freq Control*, vol. 63, no. 5, pp. 671–682, 2016. [Online]. Available: https://www.ncbi.nlm.nih.gov/pubmed/26890732

[33] "immunotherapy," https://www.cancer.gov/publications/dictionaries/cancer-terms/def/immunotherapy, accessed: 2021-04-14.

[34] Z. Hu, X. Y. Yang, Y. Liu, M. A. Morse, H. K. Lyerly, T. M. Clay, and P. Zhong, "Release of endogenous danger signals from hifu-treated tumor cells and their stimulatory effects on apcs," *Biochem Biophys Res Commun*, vol. 335, no. 1, pp. 124–31, 2005. [Online]. Available: https://www.ncbi.nlm.nih.gov/pubmed/16055092

[35] "Radiation therapy to treat cancer," https://www.cancer.gov/about-cancer/treatment/types/radiation-therapy, accessed: 2021-04-14.

[36] X. Mei, R. Ten Cate, C. M. van Leeuwen, H. M. Rodermond, L. de Leeuw, D. Dimitrakopoulou, L. J. A. Stalpers, J. Crezee, H. P. Kok, N. A. P. Franken, and A. L. Oei, "Radiosensitization by hyperthermia: The effects of temperature, sequence, and time interval in cervical cell lines," *Cancers (Basel)*, vol. 12, no. 3, 2020. [Online]. Available: https://www.ncbi.nlm.nih.gov/pubmed/32138173

[37] S. Y. Lee, G. Fiorentini, A. M. Szasz, G. Szigeti, A. Szasz, and C. A. Minnaar, "Quo vadis oncological hyperthermia (2020)?" *Front Oncol*, vol. 10, p. 1690, 2020. [Online]. Available: https://www.ncbi.nlm.nih.gov/pubmed/33014841

[38] "Glioblastoma multiforme," https://www.aans.org/en/Patients/Neurosurgical-Conditions-and-Treatments/Glioblastoma-Multiforme, accessed:

2021-04-13.

[39] K. Bilmin, T. Kujawska, and P. Grieb, "Sonodynamic therapy for gliomas. perspectives and prospects of selective sonosensitization of glioma cells," *Cells*, vol. 8, no. 11, 2019. [Online]. Available: https://www.ncbi.nlm.nih.gov/pubmed/31766152

[40] C. G. Hadjipanayis, G. Widhalm, and W. Stummer, "What is the surgical benefit of utilizing 5-aminolevulinic acid for fluorescence-guided surgery of malignant gliomas?" *Neurosurgery*, vol. 77, no. 5, pp. 663–73, 2015. [Online]. Available: https://www.ncbi.nlm.nih.gov/pubmed/26308630

[41] X, "5-aminolevulinic acid and the blood-brain barrier – a review," *Medical Laser Application*, vol. 18, no. 1, pp. 36–40, 2003. [Online]. Available: https://www.sciencedirect.com/science/article/pii/S1615161504700848

[42] C. G. Hadjipanayis, G. Widhalm, and W. Stummer, "What is the surgical benefit of utilizing 5-aminolevulinic acid for fluorescence-guided surgery of malignant gliomas?" *Neurosurgery*, vol. 77, no. 5, pp. 663–73, 2015. [Online]. Available: https://www.ncbi.nlm.nih.gov/pubmed/26308630

[43] S. G. Zhao, X. F. Chen, L. G. Wang, G. Yang, D. Y. Han, L. Teng, M. C. Yang, D. Y. Wang, C. Shi, Y. H. Liu, B. J. Zheng, C. B. Shi, X. Gao, and N. G. Rainov, "Increased expression of abcb6 enhances protoporphyrin ix accumulation and photodynamic effect in human glioma," *Ann Surg Oncol*, vol. 20, no. 13, pp. 4379–88, 2013. [Online]. Available: https://www.ncbi.nlm.nih.gov/pubmed/22688660

[44] P. C. Krishnamurthy, G. Du, Y. Fukuda, D. Sun, J. Sampath, K. E. Mercer, J. Wang, B. Sosa-Pineda, K. G. Murti, and J. D. Schuetz, "Identification of a mammalian mitochondrial porphyrin transporter," *Nature*, vol. 443, no. 7111, pp. 586–9, 2006. [Online]. Available: https:

//www.ncbi.nlm.nih.gov/pubmed/17006453

[45] W. Stummer, J. C. Tonn, C. Goetz, W. Ullrich, H. Stepp, A. Bink, T. Pietsch, and U. Pichlmeier, "5-aminolevulinic acid-derived tumor fluorescence: the diagnostic accuracy of visible fluorescence qualities as corroborated by spectrometry and histology and postoperative imaging," *Neurosurgery*, vol. 74, no. 3, pp. 310–9; discussion 319–20, 2014. [Online]. Available: https://www.ncbi.nlm.nih.gov/pubmed/24335821

[46] *StatPearls*, 2021. [Online]. Available: https://www.ncbi.nlm.nih.gov/pubmed/30726014

[47] M. E. Koller and I. Romslo, "Studies on the uptake of porphyrin by isolated rat liver mitochondria," *Biochim Biophys Acta*, vol. 503, no. 2, pp. 238–50, 1978. [Online]. Available: https://www.ncbi.nlm.nih.gov/pubmed/687606

[48] N. Rebeiz, S. Arkins, K. W. Kelley, and C. A. Rebeiz, "Enhancement of coproporphyrinogen iii transport into isolated transformed leukocyte mitochondria by atp," *Arch Biochem Biophys*, vol. 333, no. 2, pp. 475–81, 1996. [Online]. Available: https://www.ncbi.nlm.nih.gov/pubmed/8809089

[49] S. K. Wu, M. A. Santos, S. L. Marcus, and K. Hynynen, "Mr-guided focused ultrasound facilitates sonodynamic therapy with 5-aminolevulinic acid in a rat glioma model," *Sci Rep*, vol. 9, no. 1, p. 10465, 2019. [Online]. Available: https://www.ncbi.nlm.nih.gov/pubmed/31320671

[50] M. Lara-Velazquez, R. Al-Kharboosh, S. Jeanneret, C. Vazquez-Ramos, D. Mahato, D. Tavanaiepour, G. Rahmathulla, and A. Quinones-Hinojosa, "Advances in brain tumor surgery for glioblastoma in adults," *Brain Sci*, vol. 7, no. 12, 2017. [Online]. Available: https://www.ncbi.nlm.nih.gov/pubmed/29261148

[51] E. Angeli, T. T. Nguyen, A. Janin, and G. Bousquet, "How to

make anticancer drugs cross the blood-brain barrier to treat brain metastases," *Int J Mol Sci*, vol. 21, no. 1, 2019. [Online]. Available: https://www.ncbi.nlm.nih.gov/pubmed/31861465

[52] "Essential tremor," https://www.fusfoundation.org/diseases-and-conditions/neurological/essential-tremor, accessed: 2021-04-20.

[53] "Parkinson's disease," https://www.fusfoundation.org/diseases-and-conditions/neurological/parkinsons-disease, accessed: 2021-04-20.

[54] "Exablate blood-brain barrier (bbb) disruption for the treatment of alzheimer's disease," https://clinicaltrials.gov/ct2/show/NCT03671889?term=NCT03671889&rank=1, accessed: 2021-05-04.

[55] N. McDannold, G. T. Clement, P. Black, F. Jolesz, and K. Hynynen, "Transcranial magnetic resonance imaging- guided focused ultrasound surgery of brain tumors: initial findings in 3 patients," *Neurosurgery*, vol. 66, no. 2, pp. 323–32; discussion 332, 2010. [Online]. Available: https://www.ncbi.nlm.nih.gov/pubmed/20087132

[56] Y. S. Hsiao, R. E. Kumon, and C. X. Deng, "Characterization of lesion formation and bubble activities during high intensity focused ultrasound ablation using temperature-derived parameters," *Infrared Phys Technol*, vol. 60, pp. 108–117, 2013. [Online]. Available: https://www.ncbi.nlm.nih.gov/pubmed/23878517

[57] G. Y. Wan, Y. Liu, B. W. Chen, Y. Y. Liu, Y. S. Wang, and N. Zhang, "Recent advances of sonodynamic therapy in cancer treatment," *Cancer Biol Med*, vol. 13, no. 3, pp. 325–338, 2016. [Online]. Available: https://www.ncbi.nlm.nih.gov/pubmed/27807500

[58] "When is ultrasound used vs. an mri for bone, muscle and joint problems?" https://health.clevelandclinic.org/when-is-ultrasound-used-vs-an-mri-for-bone-muscle-and-joint-problems/, accessed: 2021-04-21.

[59] R. Spector, S. Robert Snodgrass, and C. E. Johanson, "A balanced view of the cerebrospinal fluid composition and functions: Focus on adult humans," *Exp Neurol*, vol. 273, pp. 57–68, 2015. [Online]. Available: https://www.ncbi.nlm.nih.gov/pubmed/26247808

[60] "Increased intracranial pressure: What to know," https://www.medicalnewstoday.com/articles/, accessed: 2021-04-14.

[61] "5 types of pressure sensors you should know," https://www.gemssensors.com/blog/blog-details/5-types-pressure-sensors-know, accessed: 2021-04-14.

[62] "Piezoresistive pressure sensors," https://www.avnet.com/wps/portal/abacus/solutions/technologies/sensors/pressure-sensors/core-technologies/piezoresistive-strain-gauge/, accessed: 2021-04-14.

[63] A. A. Barlian, W. T. Park, J. R. Mallon, A. J. Rastegar, and B. L. Pruitt, "Review: Semiconductor piezoresistance for microsystems," *Proc IEEE Inst Electr Electron Eng*, vol. 97, no. 3, pp. 513–552, 2009. [Online]. Available: https://www.ncbi.nlm.nih.gov/pubmed/20198118

[64] M. T. Chorsi, E. J. Curry, H. T. Chorsi, R. Das, J. Baroody, P. K. Purohit, H. Ilies, and T. D. Nguyen, "Piezoelectric biomaterials for sensors and actuators," *Adv Mater*, vol. 31, no. 1, p. e1802084, 2019. [Online]. Available: https://www.ncbi.nlm.nih.gov/pubmed/30294947

[65] Z. L. Wang, "Progress in piezotronics and piezo-phototronics," *Adv Mater*, vol. 24, no. 34, pp. 4632–46, 2012. [Online]. Available: https://www.ncbi.nlm.nih.gov/pubmed/22331639

[66] "Icp monitoring," https://www.integralife.com/cerelink-icp-monitoring-system/category/advanced-monitoring-cerelink-icp-monitoring-system, accessed: 2021-04-14.

[67]

[68] "Capacitive vs piezoresistive vs piezoelectric pressure sensors," https://www.avnet.com/wps/portal/abacus/solutions/technologies/sensors/pressure-sensors/core-technologies/capacitive-vs-piezoresistive-vs-piezoelectric/, accessed: 2021-04-22.

[69] "Optical fiber tutorial - optic fiber - communication fiber," https://www.fiberoptics4sale.com/blogs/archive-posts/95146054-optical-fiber-tutorial-optic-fiber-communication-fiber, accessed: 2021-04-14.

[70] "Medical pressure monitoring," https://fiso.com/wp-content/uploads/2018/10/MC-00263_-Medical-Pressure-Monitoring-Product-Datasheet_R7/, accessed: 2021-04-14.

TARANA PARVEZ KAOVASIA

2440 St. Paul Street, Astor Court, Baltimore, MD 21218 | +1 (443) 5272736 | tkaovas1@jhu.edu

EDUCATION

Johns Hopkins University, Whiting School of Engineering — Baltimore, MD
Master of Science and Engineering in Biomedical Engineering — (Expected May 2021)
GPA: 3.86/4.00

SRM Institute of Science and Technology — Chennai, India
Bachelor of Technology in Electrical and Electronics Engineering — (2015-2019)
GPA: 9.35/10.00, Silver Medal

RESEARCH EXPERIENCE

Center for Neuro-Acoustic Technologies (Manbachi Lab), Johns Hopkins Medicine (Dec 2019 – Present)

- Application of Focused Ultrasound in Sonodynamic Therapy for the treatment of Glioblastoma Multiforme (GBM) – *In Progress*
  Collaboration with the JHMI Hunterian Laboratory
  - Preparation of co-cultures for in-vitro studies
  - Rat GBM model preparation (tumor implantation and tail-vein catheterization) for the in-vivo studies
  - Using the RK300 to perform MRI-guided focused ultrasound (single-point, multi-point, and multiple-treatment)
  - Measuring the effect of the treatment on tumor volume, survival time, CSF pressure
- Design of the Acute CSF Management Implant (ACMI), HEPIUS System of Systems (DARPA Grant) – *In Progress*
  Collaboration: JHU Applied Physics Laboratory
  - Schematic design of the ACMI's pressure sensor
  - Preliminary and critical design review of the ACMI's pressure sensor
  - Complete hardware prototype of the implant
  - Design of the experimental setup for proof of concept verification of the prototype
- Ultrasound Imaging to detect and subsequently prevent cotton ball retention in neurosurgery
  - Porcine cadaver ex-vivo studies to detect cotton balls of various sizes and at various depths of the brain parenchyma
  - CAD (using SolidWorks) and 3D printing (using the Object) of a depth dox
  - Using the Clarius and Butterfly ultrasound probes to collect B-mode images
- Design of a custom 3D printed ultrasound probe holder to reduce noise induced by handheld movement – *In Progress*
  - CAD (using COMSOL) and 3D printing of the probe holder
  - Animal (porcine) translational studies to validate the improvement in image quality on imaging with the probe holder

SMARTS Lab, Johns Hopkins University (Sept 2019 – Feb 2020)
Instrument Tip Force Measurement & Verification for Application in Surgical Robotics

- Built the entire experimental setup that included two force sensors and a UR3 Arm
- Collected and analyzed data from the two sensors to verify the estimated forces at the tool tip and phantom-end using ROS and MATLAB

TEACHING AND ADMINISTRATIVE EXPERIENCE

Teaching Assistant (Jan 2021 – present)
Applied Bioelectrical Engineering, Department of Biomedical Engineering, Johns Hopkins University

- Conduct office hours to assist students with understanding concepts of the course
- Assist the professor with designing questions for the group discussions, homeworks and quizzes

Teaching Assistant (Sept 2020 – Dec 2020)
Principles of Design of Biomedical Instrumentation, Department of Biomedical Engineering, Johns Hopkins University

- Designed and graded the lab component of the course
- Performed remote demonstration of the labs and sample projects
- Conducted lab hours and office hours to assist students with the lab (remote debugging) and theory component of the course

Graduate Assistant (Jan 2020- Apr 2020)
Centre for Diversity & Inclusion, Johns Hopkins University

- Organized logistics and analyzed data for the Identity & Inclusion Workshops

PROJECTS

Bio-Gaming Control for Bilateral Below-Elbow Amputees (Nov 2019)

- Wrote a microcontroller-based algorithm to implement keystroke based on inputs from multiple sensors
- Assembled and integrated all electrical components into the system

Control Scheme Implementation on a UR5 Arm for Home to Target Configuration Transition (Nov 2019)

- Implemented the Gradient-based control scheme using MATLAB and ROS

Wearable Foetal Activity Counter (Oct 2019)

- Designed a microcontroller-based system using the piezo transducers as the sensors
- Assembled and integrated all the components into the system

A Mechanism Using Shape-Memory Alloys to Assist Affected Limb Motion in Partially Paralyzed Patients (Sept 2018 – May 2019)

- Framed the outline of the entire mechanism and simulated the required joint angles in OpenSim 4.0
- Designed the entire electronic interface and integrated it into the mechanism

Team SRMSAT - Design of a Micro-class Satellite to be Launched into Space (Aug 2016 – May 2019)

- Designed and implemented a robust Attitude Control System to achieve the desired pointing accuracy required by the spacecraft during its various functional and operational modes in MATLAB Simulink

Electrical Reconfiguration of a Partially Shaded P.V. System Using Proposed Intelligent Series Inducing Switching (Feb – Apr 2018)

- Designed the switching method to electrically configure PV panels that optimizes power output during partial panel-shading
- Simulated the system using MATLAB Simulink

PUBLICATIONS

- Smruti Mahapatra et al, **'Automatic detection of cotton balls during brain surgery: where deep learning meets ultrasound imaging to tackle foreign objects'**, Proc. SPIE 11602, Medical Imaging 2021: Ultrasonic Imaging and Tomography, 116021C (26 February 2021); DOI: 10.1117/12.2580887
- Tarana Parvez Kaovasia, Siddharth Dash, **'A novel portable device used to perform autologous blood transfusion in an unsterilized environment'**, 4th World Congress on New Technologies, ICBB'18, August 19-21, 2018. DOI: 10.11159/icbb18.103
- Tarana Parvez Kaovasia, Siddharth Dash, '**A mechanism using shape-memory alloys to assist partially paralyzed patients in walking with a natural gait***',* 4th World Congress on New Technologies, ICBB'18, August 19-21, 2018. DOI: 10.11159/icbb18.105
- A Geetha et al**, Electrical Power Generation and Storage System in Electric Vehicle–An Overview***,* International Journal for Control Theory and Application, I J C T A, 9(10), 2016, pp. 453-461

TECHNICAL SKILLS

- Software: MATLAB Simulink, COMSOL, PSPICE, LabVIEW, AutoCAD, TINA, Arduino, SolidWorks, Fusion360, 3D Slicer
- Design: PCB Fabrication, 3D Printing
- Programming Language: MATLAB, C++, ROS, Python

HACKATHONS

- FixingBad, **HopHacks**, Johns Hopkins University (Sept 2020)
  - Prototyped a simple website that is operable by the average user and directly validates information about COVID-19 without producing confusing results
  - Achievements: Hacking- Runner Up, Best Use of Google Cloud - COVID-19 Hackathon Fund, Winners of DigitalOcean, Best Application to Support Philanthropic Goals (Bloomberg)
  - Devpost link: https://devpost.com/software/fixing-facts-5iks7x
- FireHacker, **MedHacks**, Johns Hopkins University (Sept 2020)
  - Prototyped a sensor-based approach to alert older individual's about unattended cooking stoves
  - Devpost link: https://devpost.com/software/fire-hacker
- COVID-19 Risk Assessment Tool, **COVID-19 Design Challenge**, Johns Hopkins University (Mar 2020)
  - Prototyped an app using a real-time risk assessment model coupled with human traffic monitoring

INTERSHIPS

Winter Intern **(**Dec 2017)
Cummins India Office Pune, India

- Observed and learned the various aspects of Wiring Harness Systems as used in automobiles

Product Test Intern **(**Jun - July 2016)
EMI/EMC Lab, Research Centre Imarat, DRDO Hyderabad, India

- Gained first-hand experience of industrial grade product testing and defence-based projects

LEADERSHIP SKILLS

- **Member -** LGBTQA Graduate Advisory Board, Johns Hopkins University (2020 – Present)
- **Organizer -** The Quality Assurance Committee, Aaruush'18, SRMIST (2018 – 2019)
- **Joint Secretary -** EEE Association, SRMIST (2017 – 2018)
- **Soccer Representative -** Represented Maharashtra in soccer at the 56th and 57th National School Games (2010 – 2012)

SCHOLARSHIPS

- 25th Anniversary FEZANA Endowed Scholarship for Excellence (2020-2021)
- Vakhshoori Foundation Scholarship (2019-2020)
- R.D. Sethna Scholarship Awardee (2019-2020)
- Performance-based Scholarship, SRMIST (2015-16, 2016-2017, 2017-18)

Biographical sketch

Tarana was born in Mumbai and brought up in Pune, India. Growing up, her family played an important role in exposing her to a variety of experiences, in addition to supporting her in endeavours of her own. This is the primary reason why she has played soccer at a national level along with training in piano, swimming, horse-back riding and roller skating. The importance of working towards achieving what she wanted was imbibed into her from the very beginning.

She is interested in the design and development of devices and therapies to augment the healthcare system through innovation and the application of new technologies. With a background in Electrical and Electronics Engineering, she is pursuing her Master's in Biomedical Engineering at Johns Hopkins University. Her current research is in the field of focused ultrasound and smart sensing. After graduating, she will be continuing her research in the field of focused ultrasound during her Ph.D. studies.